RESEARCH ARTICLE SUMMARY

DEVELOPMENT

Patterns of brain-wide associations reflect socioeconomics

Scott Marek* *et al.*

Full article and list of author affiliations:
https://doi.org/10.1126/science.aee6213

INTRODUCTION: Brain-wide association studies (BWAS) link individual differences in behavioral traits [e.g., intelligence quotient (IQ)] or living conditions (e.g., socioeconomic status) to variability in our brain function and structure. Widely used BWAS measures include magnetic resonance imaging (MRI)–derived resting-state functional connectivity, which successfully maps networks based on spontaneous neural fluctuations, and cortical thickness. Prior BWAS have associated brain imaging data with single traits, most commonly IQ or psychopathology, prioritizing association strength over spatial patterns. Although large samples improve BWAS replicability, the relative importance of different environmental and behavioral variables, their relationships to each other, and the interpretation of the underlying brain patterns remain unclear.

RATIONALE: Datasets with many thousands of participants enable us to simultaneously map hundreds of nonimaging variables to the brain and to compare them both with each other and with well-established neurobiological reference patterns (non-BWAS). This framework leverages existing knowledge of brain biology for abductive pattern-based inference. For example, higher-order cognition relies on the frontal and parietal cortices, whereas the effects of sleep deprivation and stress manifest in primary motor and sensory regions. With such neurobiological patterns as a guiding light, we can robustly infer meaning from the BWAS patterns and identify which brain-wide associations may reflect confounding or are only valid for certain subsets of people.

RESULTS: Across 649 nonimaging variables, in a large sample of 9 to 10 year olds, socioeconomic measures had the strongest and most replicable brain-wide associations. The single strongest brain association was with the socioeconomic opportunities afforded by a child's zip code. This socioeconomic brain pattern was dominant and permeated many of the other BWAS maps. Socioeconomic associations were concentrated in primary motor and sensory regions, with strong spatial similarity to arousal and stress patterns, including norepinephrine receptor density, sleep duration, and stimulant medication effects, while being negatively correlated with task functional MRI maps of higher-order cognition. Unexpectedly, the BWAS map of IQ closely matched the socioeconomic pattern. Adjusting for socioeconomics reduced brain-IQ associations and shifted them away from arousal and toward a pattern more similar to cognition, consistent with confounding by socioeconomics. Multivariate brain-IQ models failed when trained on samples from higher socioeconomic strata lacking a correlation between socioeconomics and IQ. Brain-IQ models could only detect associations when the training sample included children from neighborhoods with lower socioeconomic status. However, these were misleading, because the IQ-trained models still predicted socioeconomics better than IQ, consistent with shortcut learning.

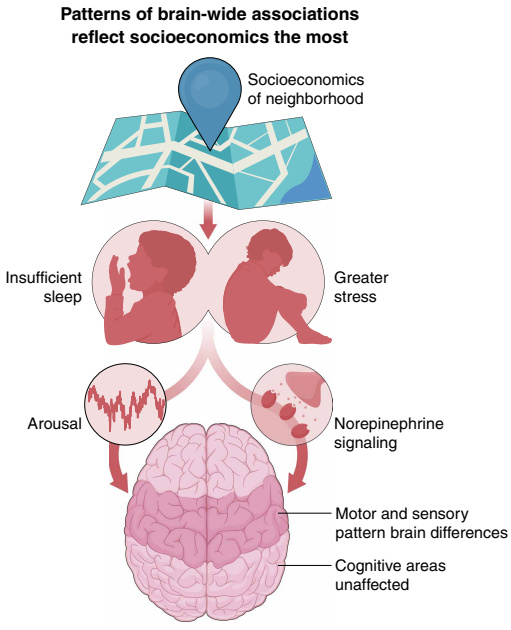

Socioeconomics is the dominant axis of childhood brain organization. Brain-wide associations in the Adolescent Brain Cognitive Development (ABCD) Study revealed that socioeconomic status exhibited the strongest associations with brain organization. Socioeconomic status dominated population-level variation through arousal-related patterns linked to sleep and stress, specifically norepinephrine and stimulant effect maps. Socioeconomic status models demonstrated robust generalizability across different groups, highlighting its importance as the primary variable in childhood BWAS. [Figure created by Lucy Reading-Ikkanda]

CONCLUSION: Socioeconomic circumstances are more powerfully associated with brain function and structure than other variables. The dominant socioeconomic brain pattern matches the known effects of sleep deprivation and stress (primary motor and sensory) while sparing higher-order cognitive regions in the frontal and parietal cortices. Thus, it appears most likely that environmental factors indexed by neighborhood socioeconomic status, including sleep and stress, strongly shape childhood brain organization. This stands in contrast to brain-IQ associations that are confounded and reflect shortcut learning of socioeconomics rather than brain-based differences. Accounting for socioeconomics improves BWAS interpretation and generalizability. In summary, neighborhood socioeconomics represent the principal axis shaping brain organization during childhood and beyond, potentially through sleep and stress. □

*Corresponding author. Email: smarek@wustl.edu Cite this article as S. Marek *et al.*, *Science* **392**, eaee6213 (2026). DOI: 10.1126/science.aee6213

DEVELOPMENT

Patterns of brain-wide associations reflect socioeconomics

Scott Marek[1,2,3,4,5]*, Meghan Rose Donohue[4], Nicole R. Karcher[4], Caroline P. Hoyniak[4], Roselyne J. Chauvin[1,2,6], Ashley C. Meyer[1,2,3], John Miller[1,2,3], Andrew N. Van[2,3,6], Anxu Wang[2,3,6], Noah J. Baden[2,3,6], Vahdeta Suljic[2,3,6], Kristen M. Scheidter[2,3,6], Julia Monk[2,3,6], Forrest I. Whiting[2,3,6], Nadeshka J. Ramirez-Perez[2,3,6], Samuel R. Krimmel[2,3,6], Athanasia Metoki[2,3,6], Sarah E. Paul[7], Aaron J. Gorelik[7], Timothy J. Hendrickson[8], Stephen M. Malone[9], Rebecca F. Schwarzlose[3,4], Carlos Cardenas-Iniguez[10], Megan M. Herting[10], Steven E. Petersen[1,3,7,11], Joan Luby[4], Anita C. Randolph[12,13], Michael J. Shanahan[14,15], Eric Turkheimer[16], Benjamin P. Kay[2,3,6], Evan M. Gordon[1,2,3], Timothy O. Laumann[2,3,4], Deanna M. Barch[4,7], Damien A. Fair[12,17,18], Brenden Tervo-Clemmens[12,13,19], Nico U. F. Dosenbach[1,2,3,6,7,20,21,22]

Previous brain-wide association studies (BWAS) have linked specific environmental and behavioral variables to brain variability. In this work, we mapped 649 variables to children's brains and compared the resultant BWAS maps with each other and with neurobiological reference patterns. Socioeconomic status (SES) showed the strongest brain-wide associations. The SES associations were strongest in motor and sensory but not cognitive regions, a pattern shared across many BWAS maps, including intelligence quotient (IQ). A single, common BWAS brain pattern existed across variables that was most reflective of a child's socioeconomics. Adjusting for SES weakened brain-IQ associations, eliminating the BWAS motor and sensory pattern. Brain-with-IQ associations also did not generalize when trained on higher-SES subsamples. Thus, children's brains vary the most with SES, potentially through SES-dependent sleep deprivation and stress.

Brain-wide association studies (BWAS) link behavioral or environmental variability to measures of brain function or structure (*1*–*3*) across people. Despite growing sample sizes and increasingly sophisticated analytics (*4*–*6*), neurophysiological interpretability and generalizability of BWAS associations have remained limited. Recent large-population datasets (*7*, *8*) now enable replicable BWAS mapping across a large swath of environmental exposures (exposome) and observable traits (phenome), which allows for comparison with brain data from other modalities. Identifying patterns that recur across hundreds of variables may reveal shared neurobiological processes, thereby enhancing BWAS interpretation.

Resting-state functional connectivity (RSFC) and cortical thickness are among the most widely used neuroimaging measures of human brain function and structure, respectively. Both are straightforward to acquire, are stable within individuals (*9*, *10*) [given sufficient quality data (*11*)], and display substantial interindividual variability. Spontaneous neural fluctuations (RSFC) are correlated in systematic ways (*12*–*14*), organizing the brain into approximately a dozen canonical networks based on their functions (*11*, *15*, *16*). Sensory and motor networks show relatively greater day-to-day RSFC variability (*9*, *17*) and sensitivity to stress, arousal (*18*), and drowsiness (*19*). Conversely, the frontoparietal network (FPN) is more stable day-to-day (*17*, *20*) and supports highest-order abstract cognitive processes (*21*)—for example, logic and mathematics (*22*, *23*). Effect sizes for cortical thickness are smaller than those for RSFC (*1*), but cortical thickness has been reliably linked with development (*24*), aging (*25*), socioeconomic status (SES) (*26*), and mental health (*26*, *27*).

Previous BWAS have typically focused on a single cognitive or clinical variable, most commonly intelligence quotient (IQ) (g; Fig. 1A) or total psychopathology (p-factor; Fig. 1B). However, brain function and structure are known to be affected by extreme environmental exposures, such as childhood abuse (*28*–*32*) and neglect (*33*–*35*), institutional care (*36*, *37*), and poverty (*38*), which confer increased risk for psychopathology and cognitive difficulties (*28*, *39*). The extent to which typical environments might affect the interpretability and generalizability of common BWAS findings remains unclear. Assessing the relative contribution of brain biology and environment to phenotypic traits is critical for interpreting BWAS.

In this work, we mapped 649 variables (exposome + phenome) (*40*) to RSFC and cortical thickness in the Adolescent Brain Cognitive Development (ABCD) Study and analyzed the principal dimension of population-level variability. We used pattern-based inference to interpret BWAS patterns by contrasting them with functional reference maps established by other methods, including positron emission tomography (PET), electroencephalography (EEG), medication effects, and task functional magnetic resonance imaging (fMRI). Additionally, we tested the generalizability of key brain-wide association patterns in multiple ways, including through evaluating their relative dependence on subsample characteristics.

Socioeconomics have the strongest brain-wide associations

The classical BWAS variables, IQ (Fig. 1A, RSFC; see fig. S1A for cortical thickness) and total psychopathology (Fig. 1B, p-factor, RSFC; see fig. S1B for cortical thickness), show distributed brain patterns, with stronger associations for IQ than for psychopathology. To cover the breadth of the exposome and phenome, we generated BWAS maps (univariate) for 649 variables in the preregistered (*41*) discovery dataset of the ABCD Study [Fig. 1C; $N = 2316$ individuals; ages 8.9 to 11 years, mean = 9.9 years, SD = 7.5 months; female:male ratio (F:M) = 52:48]. Ranking all 649 ABCD variables (table S1) by their univariate brain-wide association patterns (r_{BWAS}) from strongest to weakest revealed socioeconomics, not cognitive abilities or mental health, to be the most strongly associated with brain function and structure (see Fig. 1C for RSFC; fig. S1C for cortical thickness; fig. S2 for replication in ABCD year 2; and table S1 for all 649 variables ranked). Of the top 40 variables by association strength with RSFC, 37 were related to a child's socioeconomic environment, with the remaining three related to sleep and screen time. For cortical thickness, 35 of the top 40 variables were socioeconomic (fig. S1C). Across all 12 predefined categories,

[1]Mallinckrodt Institute of Radiology, Washington University School of Medicine, St. Louis, MO, USA. [2]Allied Labs for Imaging Guided Neurotherapies (ALIGN), Washington University School of Medicine, St. Louis, MO, USA. [3]Neuroimaging Labs Research Center, Washington University School of Medicine, St. Louis, MO, USA. [4]Department of Psychiatry, Washington University School of Medicine, St. Louis, MO, USA. [5]AI Institute for Health, Washington University School of Medicine, St. Louis, MO, USA. [6]Department of Neurology, Washington University School of Medicine, St. Louis, MO, USA. [7]Department of Psychological and Brain Sciences, Washington University in St. Louis, St. Louis, MO, USA. [8]University of Minnesota Informatics Institute, University of Minnesota, Minneapolis, MN, USA. [9]Department of Psychology, University of Minnesota, Minneapolis, MN, USA. [10]Department of Population and Public Health Sciences, Keck School of Medicine, University of Southern California, Los Angeles, CA, USA. [11]Department of Neurological Surgery, Washington University School of Medicine, St. Louis, MO, USA. [12]Masonic Institute for the Developing Brain, University of Minnesota Medical School, Minneapolis, MN, USA. [13]Department of Pediatrics, University of Minnesota Medical School, Minneapolis, MN, USA. [14]Jacobs Center for Productive Youth Development, University of Zurich, Zurich, Switzerland. [15]Institute of Sociology, University of Zurich, Zurich, Switzerland. [16]Department of Psychology, University of Virginia, Charlottesville, VA, USA. [17]Department of Psychiatry & Behavioral Sciences, University of Minnesota Medical School, Minneapolis, MN, USA. [18]Institute of Child Development, University of Minnesota Medical School, Minneapolis, MN, USA. [19]Institute for Translational Neuroscience, University of Minnesota Medical School, Minneapolis, MN, USA. [20]Program in Occupational Therapy, Washington University School of Medicine, St. Louis, MO, USA. [21]Department of Pediatrics, Washington University School of Medicine, St. Louis, MO, USA. [22]Department of Biomedical Engineering, Washington University in St. Louis, St. Louis, MO, USA. *Corresponding author. Email: smarek@wustl.edu

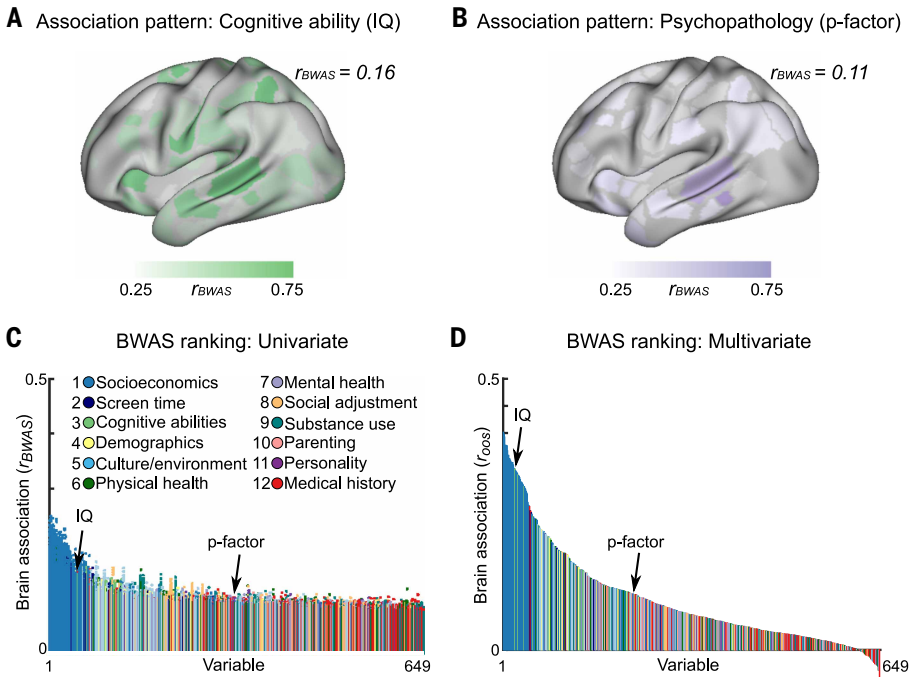

Fig. 1. BWAS strength rankings. RSFC BWAS maps (bivariate correlation, $|r_{BWAS}|$; see fig. S1, A and B, for cortical thickness) for commonly studied exemplar variables. (**A** and **B**) Cognitive ability (IQ scores; NIH Toolbox Cognition Battery, total score) (A) and psychopathology (p-factor; Child Behavior Checklist, total score) (B) in a predefined discovery ($n = 2316$; training) set of baseline ABCD data. Values in (A) and (B) are min/max (0 to 1) normed. The value displayed for r_{BWAS} is the maximum. (**C**) Brain-behavior association strength (*y* axis) for 649 nonimaging variables (*x* axis). Each colored dot (55,278 dots for each variable) represents a single association between a brain measure (RSFC edge) and a nonimaging variable (see fig. S1C for cortical thickness). Dot color represents the predefined category of the variable. The nonimaging variables (*x* axis) are ranked by their 99% CIs across all 55,278 associations. All associations were based on at least $n > 2000$ individuals. (**D**) Multivariate brain-behavior associations [bivariate correlation (r_{oos}) between out-of-sample predicted and observed scores] for all nonimaging variables, using RSFC and ridge regression (Materials and methods; see fig. S1D for cortical thickness). Models were trained on the discovery ($n = 2316$; training) set and subsequently tested on the matched (Materials and methods) left-out replication ($n = 2263$; test) set. Dot color represents the predefined category of the variable. The nonimaging variables (*x* axis) are ranked by their multivariate association strength (r_{oos}).

socioeconomics demonstrated the strongest brain-wide associations for both RSFC [$F_{11,648} = 51.42$, $P = 6.52 \times 10^{-81}$; one-way analysis of variance (ANOVA)] and cortical thickness ($F_{11,648} = 20.73$, $P = 3.54 \times 10^{-36}$) followed by screen time and cognition.

The strongest univariate brain-wide association was between the social and economic domain of the Child Opportunity Index (referred to as SES hereafter) and RSFC: maximum $r_{BWAS} = 0.24$ (for cortical thickness, $r_{BWAS} = 0.14$; seventh strongest). This RSFC with SES association was 50% stronger than the association between RSFC and IQ scores and 130% stronger than the association between RSFC and the p-factor. Rankings by effect size (r_{BWAS}) were highly similar for RSFC and cortical thickness [correlation coefficient (r) = 0.79, $P = 3.01 \times 10^{-137}$] and robust to parameter choices (Materials and methods). Moreover, rankings replicated in a matched (Materials and methods), left-out preregistered replication ABCD dataset (*41*) (RSFC: $n = 2263$, $\rho = 0.83$, $P = 5.22 \times 10^{-125}$, 37/40 top variables were socioeconomic; cortical thickness: $\rho = 0.64$, $P = 1.47 \times 10^{-77}$, 22/40 top variables were socioeconomic), a larger baseline ABCD dataset that did not exclude participants for excessive head motion (RSFC: $n = 7620$, $\rho = 0.87$, $P = 5.77 \times 10^{-196}$, 37/40 top variables were socioeconomic), and the 2 year follow-up (year 2) ABCD Study dataset (fig. S1) (RSFC: $n = 2363$, $\rho = 0.87$, 37/40 top variables were socioeconomic). Statistical adjustments for data acquisition parameters (that is, the use of different MRI scanner types across ABCD sites and the inclusion of siblings) did not alter the results (table S1 and Materials and methods).

Multivariate BWAS models yielded stronger associations (r_{oos}, out-of-sample correlation, between predicted and observed values) for RSFC (Fig. 1D) and cortical thickness (fig. S1D). The maximum multivariate brain association (ridge regression) for SES was $r_{oos} = 0.40$ for RSFC (16% of variance explained) and $r_{oos} = 0.36$ for cortical thickness. Most of the strongest multivariate associations were with socioeconomic variables (RSFC: 37/40; cortical thickness: 30/40). For RSFC and cortical thickness, the multivariate (r_{oos}) and univariate [r_{BWAS}; 99% confidence interval (99% CI)] association strengths were strongly positively correlated ($r = 0.91$ for RSFC and cortical thickness; fig. S3), underscoring that their rank order is independent of the analytic approach.

Brain-wide associations of socioeconomics are motor and sensory

The strongest brain-wide association map, that of SES with RSFC, was dominated by primary motor and sensory regions (Fig. 2A; see fig. S4A for all brain views, fig. S5A for cortical thickness, and fig. S6 for all brain views). The SES motor and sensory BWAS pattern replicated in the adult UK Biobank sample [$n = 32{,}572$ individuals, aged 40 to 69 years, 95% white British, white Irish, or other white background (*42*); fig. S7], indicating that the socioeconomic brain pattern persists in a homogeneous sample with regards to race.

The BWAS maps for other variables with strong RSFC associations, such as sleep duration ($r_{BWAS} = 0.19$; 14th strongest), screen time ($r_{BWAS} = 0.17$; 32nd strongest), and IQ scores (NIH Toolbox Cognition Battery, total score; $r_{BWAS} = 0.16$; 59th strongest) showed patterns very similar to that of SES [Fig. 2B; correlations to SES BWAS map $r_{patterns}$: ↑ sleep duration = 0.86, ↓ screen time = 0.80, ↑ IQ scores = 0.72 (all $P < 0.001$, Bonferroni-corrected, spin test) (*43*, *44*); see fig. S5, A and B, for cortical thickness], whereas the p-factor did not ($r_{patterns} = 0.29$, $P > 0.05$, Bonferroni-corrected, spin test).

Variables with BWAS patterns similar to SES also had strong direct variable-to-variable correlations with it (fig. S8A; sleep duration, $r_{vars} = 0.30$, $P = 1.27 \times 10^{-50}$; screen time, $r_{vars} = -0.24$, $P = 2.70 \times 10^{-31}$; IQ scores, $r_{vars} = 0.31$, $P = 6.78 \times 10^{-53}$; see supplementary text and fig. S8B for full r_{vars} correlation matrix). Moreover, BWAS association strengths and correlations with SES were strongly related (fig. S9, RSFC: $r = 0.87$, $P = 6.72 \times 10^{-198}$; fig. S10, cortical thickness: $r = 0.70$, $P = 2.89 \times 10^{-56}$). This relationship suggests that the p-factor may have seemingly weaker associations with the brain compared with IQ because it is more independent of SES (fig. S8A; IQ, $r_{vars} = 0.31$; p-factor, $r_{vars} = -0.09$).

To systematically compare brain patterns across all variables, we correlated the 649 BWAS maps with each other (Fig. 2C; $|r_{patterns}|$ for RSFC; see fig. S5C for cortical thickness), revealing strong spatial correlations across many socioeconomic variables (bright colors in top left of Fig. 2C for RSFC; see fig. S5C for cortical thickness). For RSFC, almost all screen time and cognition BWAS maps were strongly correlated with the SES pattern ($|r_{patterns}| > 0.50$; Fig. 2C). Across all non-socioeconomic RSFC BWAS maps, 22% were correlated at $|r_{patterns}| > 0.50$

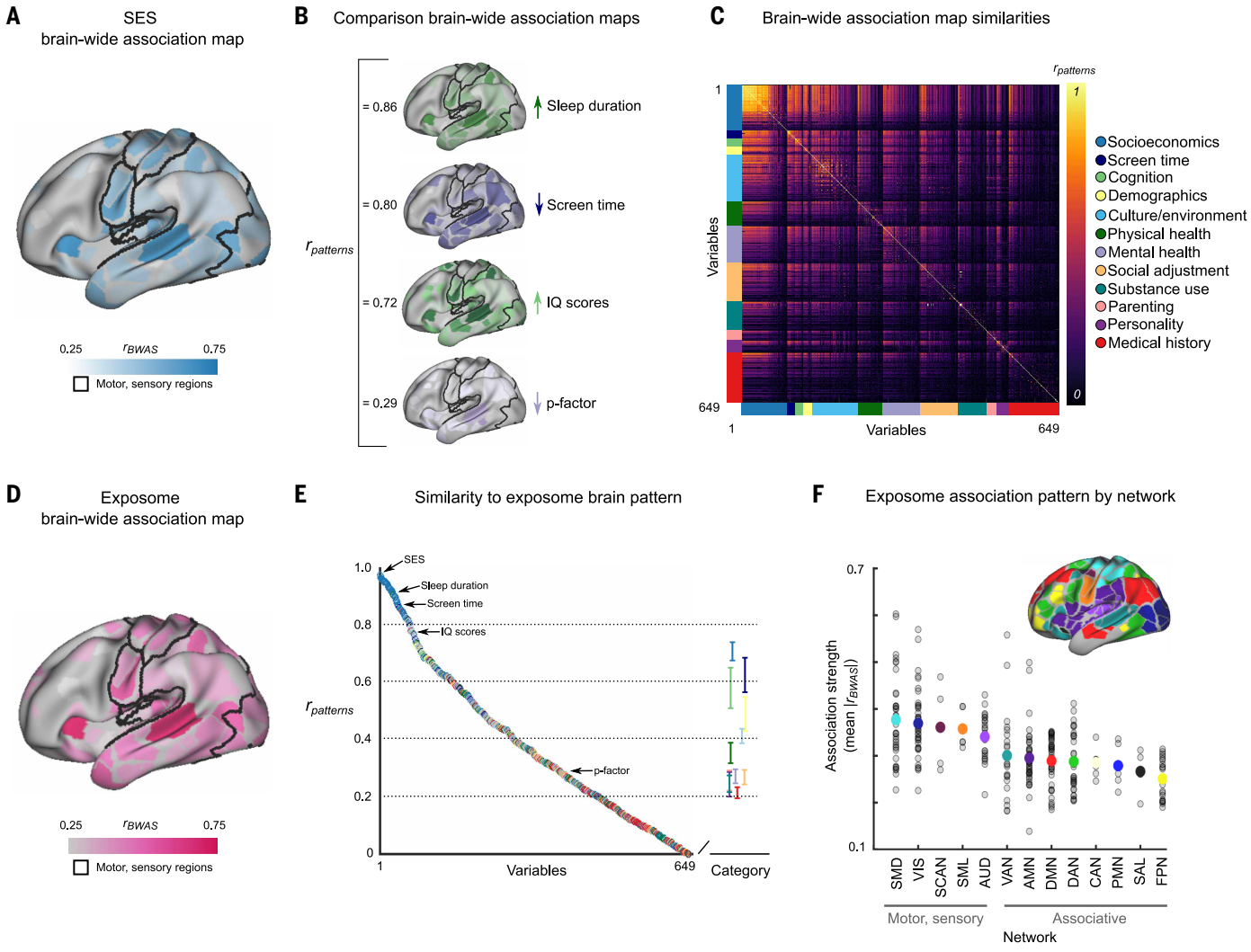

Fig. 2. BWAS map pattern analytics. (**A**) Brain-wide association map of RSFC with SES (social and economic domain of the Child Opportunity Index; see fig. S4A for medial wall and right hemisphere). Values (r_{BWAS}) are min/max (0 to 1) normed. (**B**) Exemplar brain-wide association maps for comparison (see fig. S4 for additional brain views). Bivariate correlations ($r_{patterns}$) between the maps for SES (A) and comparison maps (B) are listed in the left column of (B). (**C**) Similarity matrix depicting the correlations ($r_{patterns}$) for all possible pairs of brain-wide association maps (649 × 649). Variables are organized according to category and sorted by association strength within each category. Color tabs on the *x* and *y* axes reflect the variable categories. (**D**) The exposome map is the first PC across all 649 brain-wide association maps (see fig. S4 for additional brain views). (**E**) Correlations ($r_{patterns}$; *y* axis) of the brain-wide association maps for each variable (*x* axis) with the exposome map [from (D)]. Variables are ranked by their spatial correlation with the exposome brain-wide association map. The right side of the *x*-axis line break shows the mean ± the standard error for each category (see fig. S5 for cortical thickness). (**F**) Association strength (mean $|r_{BWAS}|$, normed; *y* axis) of the exposome map from (D) for each functional brain network (*x* axis; Materials and methods). Each gray circle represents the mean association strength ($|r_{BWAS}|$) for a parcel or region. The colored dot for each network represents the $|r_{BWAS}|$ across all regions within that network. SMD, somatomotor dorsal; VIS, visual; SML, somatomotor lateral; AUD, auditory; VAN, ventral attention; AMN, action mode; DMN, default mode; DAN, dorsal attention; CAN, context association; PMN, parietal memory; SAL, salience.

with the pattern for SES (Fig. 2C), whereas 3% of all nonsocioeconomic cortical thickness BWAS maps were correlated at $|r_{patterns}| > 0.50$ with the SES pattern (fig. S5C).

The strong neuroanatomical similarity between many BWAS maps suggested that a common association pattern may exist across variables. Thus, we extracted the first principal component (PC) of all BWAS maps (Materials and methods). The resulting principal RSFC association map (Fig. 2D; see fig. S5F for all brain views) accounted for 34% of the variance across all 649 RSFC BWAS maps (for cortical thickness, see fig. S5D; 17% for cortical thickness) and was nearly identical (PC_1 $r_{patterns}$ = 0.97) to the SES BWAS map (Fig. 2A). Given that the very strong overlap with the SES map was specific to PC_1 for both RSFC ($r_{patterns}$: $PC_2 = 0.07$, $PC_3 = 0.06$; fig. S11) and cortical thickness ($r_{patterns}$: $PC_1 = 0.94$, $PC_2 = -0.06$, $PC_3 = 0.05$), it will be referred to as the exposome map hereafter. Some of the overlap between the exposome (Fig. 2D) and the SES (Fig. 2A) brain maps could be driven by including socioeconomics when generating the exposome map. Therefore, we recomputed the exposome map after excluding all socioeconomic variables. Doing so generated a nearly identical exposome map compared with the one that also included socioeconomic variables ($r_{patterns}$ = 0.99). In summary, a single, common BWAS brain pattern existed across hundreds of variables that was most reflective of a child's socioeconomics.

To further examine the exposome map's projection onto variable-specific BWAS maps, we correlated it with each of them (Fig. 2E, $|r_{patterns}|$; see fig. S5E for cortical thickness). Socioeconomic variables,

on average, exhibited the strongest spatial similarity (median across all variables $|r_{patterns}|$: RSFC = 0.84, cortical thickness = 0.70) to the exposome association map. Across categories, measures of screen time (median $|r_{patterns}|$: RSFC = 0.67, cortical thickness = 0.42) and cognition (median $|r_{patterns}|$: RSFC = 0.66, cortical thickness = 0.49) also demonstrated relatively strong similarity to the exposome map. Considering the exemplar variables with strong brain associations (SES, sleep, screen time, and IQ) simultaneously in a multiple regression model (adjusting for age, sex, head motion, and site; Materials and methods) did not alter their BWAS similarity ranking relative to the exposome association map (Materials and methods; see fig. S12A for association strength rankings and fig. S12, B to E, for residualized brain maps of SES, sleep, screen time, and IQ).

The brain networks most strongly represented in the exposome BWAS pattern were early sensory (visual and auditory), motor (somatomotor dorsal and somatomotor lateral), and the somato-cognitive action network (SCAN) (*45*, *46*) recently discovered in the primary motor cortex (Fig. 2F; see fig. S5F for cortical thickness). Early sensory and motor networks had significantly stronger associations with the exposome map than associative networks ($t = 9.67$, $P = 2.5 \times 10^{-19}$, one-tailed independent samples t test across networks) for RSFC but not for cortical thickness (fig. S5F). The FPN (yellow) (*47*), preferentially activated during complex cognition and linked to interindividual variation in fluid IQ by task fMRI (*23*, *48*), had the least overlap with the RSFC exposome pattern (Fig. 2F).

Strongest BWAS patterns reflect arousal phenomena

To further investigate the exposome association map (RSFC), we used comparative functional pattern analytics, which quantifies differences and similarities across functional brain mapping modalities (Fig. 3). We derived meta-analytic task fMRI maps (Fig. 3A, left; working memory, reasoning, cognitive control; NeuroSynth; Materials and methods), PET receptor density maps (Fig. 3A, top right; norepinephrine) (*49*, *50*) (see table S2 for other transmitters), as well as maps of sleep (Fig. 3A, middle right; EEG) (*51*, *52*), stimulant use (Fig. 3A, bottom right; on/off methlyphenidate fMRI) (*50*, *53*), SES, and IQ. We quantified their spatial correlation with the exposome map. Calculation of spatial correlations across maps revealed that task fMRI contrasts of high cognitive demand were anticorrelated with the RSFC exposome map ($r_{patterns}$: working memory = −0.15, reasoning = −0.17, cognitive control = −0.16) and significantly distinct from it [all $P < 0.05$, false discovery rate (FDR)–corrected, spin test] (*43*, *44*). By contrast, arousal variable maps were strongly correlated (all $P < 0.05$, FDR-corrected, spin test) (*43*, *44*) with the exposome map ($r_{patterns}$: norepinephrine = 0.34, sleep = 0.44, stimulants = 0.49) as were SES ($r_{patterns} = 0.97$) and IQ ($r_{patterns} = 0.78$), thus revealing the IQ BWAS pattern to be mismatched with the known functional neuroanatomy of complex cognition [Fig. 3; see fig. S13 for pairwise correlations ($r_{patterns}$) between all functional brain maps] (*48*, *54*, *55*).

To quantify how strongly each functional pattern mapped onto the brain's primary cortex, we computed the percentage of total association strength represented in motor and sensory networks relative to the rest of the brain (Fig. 3B). Complex cognitive fMRI task maps (working memory, reasoning, and cognitive control) overlapped much less with motor and sensory (~20%) compared with all other (associative) networks (Fig. 3B, gold, left). By contrast, the BWAS (SES, exposome, and IQ; Fig. 3B, BWAS, pink, middle) and arousal (norepinephrine receptor density, sleep duration, and stimulant use; Fig. 3B, arousal, red, right) maps were dominated by motor and sensory regions (~60%). A one-way ANOVA comparing cognitive tasks (Fig. 3B, gold, left), functional connectivity BWAS (Fig. 3B, pink, middle), and arousal-related maps (Fig. 3B, red, right) demonstrated that the cognition maps (task) were significantly different from the others (BWAS, arousal: $F_{2,6} = 71.79$, $P = 6.45 \times 10^{-5}$), whereas there was no statistical difference between the other sets of maps (BWAS versus arousal: $P = 0.93$, Tukey-Kramer multiple comparison–corrected). Although comparative functional pattern analytics underscored the similarity of the exposome, SES, and IQ maps with known arousal associations, it highlighted the chasm between the accepted prefrontal and parietal distribution of higher cognition (*56*) and the motor and sensory BWAS map of IQ ($r_{patterns} = 0.00$).

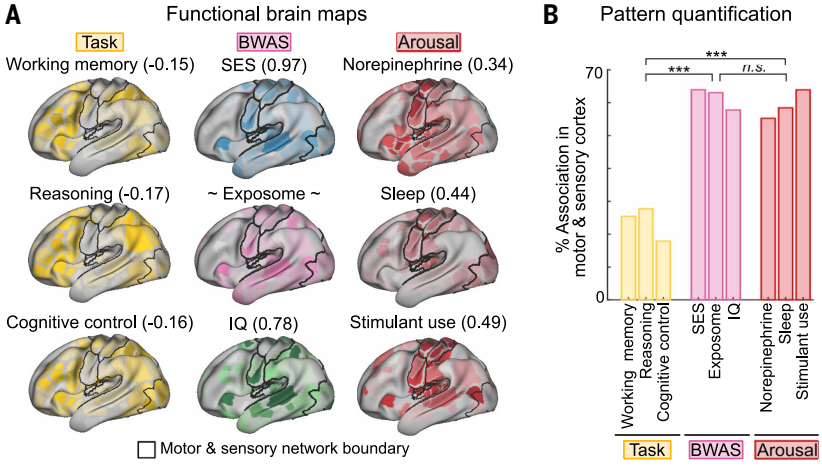

Fig. 3. Comparative functional pattern analytics. (**A**) Comparisons of task fMRI activation maps (gold, left) of higher-order cognitive tasks (working memory, reasoning, and cognitive control; NeuroSynth), RSFC BWAS maps [middle; SES (blue), exposome (pink), and IQ (green)], and non-BWAS patterns of arousal phenomena (red, right; norepinephrine receptor density, sleep duration, and stimulant use) mapped using PET (norepinephrine), EEG (sleep), and on/off methylphenidate fMRI (stimulant). The number next to each variable represents the correlation ($r_{patterns}$) of the map to the exposome BWAS map (center). Motor and sensory networks are outlined in black. All brain maps are min/max (0 to 1) normed. Color hue ranges from 0.25 (lighter) to 0.75 (deeper). (**B**) Proportion of total association represented in motor (somatomotor dorsal and lateral and somato-cognitive action) and sensory (visual and auditory) versus all other networks (associative) for higher-order cognitive tasks (gold, left; working memory, reasoning, and cognitive control; NeuroSynth), functional connectivity BWAS maps (pink, middle; SES, exposome, and IQ), and arousal phenomena (red, right; norepinephrine receptor density, sleep, and stimulant use). ***$P < 0.001$, Bonferroni-corrected; n.s., not significant ($P > 0.05$, one-way ANOVA).

Brain-IQ associations are confounded by SES

It is well known from task fMRI and other methods (lesion mapping, electrophysiology, and computational modeling) (*57*, *58*) that higher-order cognition, such as reasoning, localizes to the prefrontal and parietal cortices (Fig. 3A, left). Although IQ is considered a latent index of cognitive abilities, its BWAS pattern consisted of motor and sensory—not prefrontal and parietal—regions (Fig. 3A, middle). One potential explanation for the BWAS IQ map not matching the known pattern of higher-order cognition is that it might be confounded by SES.

If SES was confounding brain-IQ associations, then adjusting for SES by linear regression should weaken the brain-IQ association and change the BWAS pattern from motor and sensory to one more consistent with higher-order cognition (supplementary text, section "Confounding vs. Colliding," and fig. S32). Therefore, we regressed SES from IQ scores and recomputed univariate brain-wide associations with IQ (see Fig. 4, A and B, for RSFC; fig. S14 for cortical thickness; and Materials

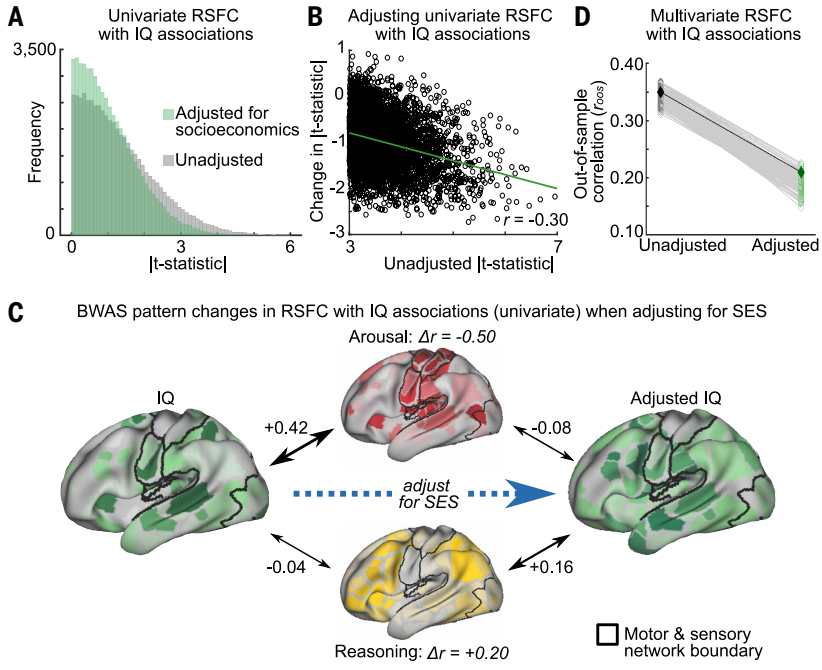

Fig. 4. Adjusting for SES in brain-IQ associations. (**A**) Distribution of associations between RSFC edges and IQ scores (NIH Toolbox Cognition Battery, total score; see fig. S14A for cortical thickness) in univariate models unadjusted for SES (gray; social and economic domain from the Child Opportunity Index) and after adjusting for SES (green) in the discovery sample ($n = 2316$). (**B**) Univariate associations of RSFC with IQ after SES adjustment (*y* axis), as a function of the unadjusted associations (*x* axis; see fig. S14B for cortical thickness). The negative slope ($r = -0.30$) indicates that adjusting for SES reduces stronger RSFC with IQ associations the most. (**C**) Comparison of IQ BWAS maps (RSFC; green) unadjusted for SES (left) and adjusted for SES (right), with arousal (on/off methylphenidate; top, red) and cognition (reasoning task fMRI; bottom, yellow). All brain maps are min/max (0 to 1) normed. Color hue ranges from 0.25 (lighter) to 0.75 (deeper). Values next to double-headed arrows represent spatial correlation ($r_{patterns}$) between brain maps. Motor and sensory networks are outlined in black. (**D**) Multivariate associations (out-of-sample: r_{oos}) of RSFC with IQ scores (see fig. S14C for cortical thickness) using ridge regression [see figs. S15 and S16 for replication with CPM (*60*)] unadjusted (gray, left) for SES and adjusted for SES (green, right). Training and testing used 100 split-half bootstraps. Black diamond (left) shows out-of-sample model fit (r_{oos}) unadjusted for SES from the predefined replication sample ($n = 2263$; Materials and methods), and green diamond (right) shows r_{oos} adjusted for SES in the same sample (Materials and methods).

and methods). Adjusting for SES weakened 95% of the brain-IQ associations for both RSFC and cortical thickness, such that ~70% of them were no longer statistically significant, whereas only 5% did not decrease and remained significant ($P < 0.001$, one-sided, mixed effect models; Fig. 4A). The strongest associations between the brain and IQ systematically decreased the most when adjusting for SES (Fig. 4B; see fig. S14B for cortical thickness).

Adjusting the IQ BWAS map for SES eliminated its similarity with the motor and sensory (stimulant) pattern, reducing it from unadjusted $r_{patterns} = 0.42$ to adjusted $r_{patterns} = -0.08$ (not significant: $\Delta r_{patterns} = -0.50$; Fig. 4C, RSFC). Simultaneously, the IQ BWAS map's similarity to the frontoparietal cognition pattern was increased from unadjusted $r_{patterns} = -0.04$ to adjusted $r_{patterns} = 0.16$ ($P = 0.045$, spin test, $\Delta r_{patterns} = +0.20$; Fig. 4C, RSFC). After adjusting for SES, the IQ BWAS pattern was more aligned with task fMRI of cognitively demanding tasks ($r_{patterns} = 0.16$) compared with arousal ($r_{patterns} = -0.08$).

Multivariate brain-IQ associations [Fig. 4D; RSFC: $r_{oos} = 0.36$, consistent with prior studies (*59*); cortical thickness: $r_{oos} = 0.23$] were reduced by 30 to 40% after SES adjustment (RSFC: $r_{oos} = 0.23$; Fig. 4D; cortical thickness: $r_{oos} = 0.13$; fig. S14C) [for replication using connectome-based predictive modeling (CPM) (*60*), see figs. S15 and S16]. Multivariate RSFC-SES associations were only reduced by ~20% when adjusting for IQ (RSFC: unadjusted for IQ $r_{oos} = 0.39$, adjusted for IQ $r_{oos} = 0.31$; cortical thickness: unadjusted for IQ $r_{oos} = 0.38$, adjusted for IQ $r_{oos} = 0.34$; fig. S17) and were similar to brain-based multivariate associations of IQ without SES adjustment ($r_{oos} = 0.32$). Confound isolation cross-validation (*61*), which tests multivariate models on subsamples of the test set without a linear association between IQ and SES, similarly showed SES to have stronger RSFC associations ($r_{oos} = 0.30$) than IQ ($r_{oos} = 0.24$; fig. S18 and Materials and methods).

Adjusting IQ BWAS for SES weakened the associations, independent of the methodology. Moreover, the SES-adjusted IQ BWAS pattern no longer overlapped with maps of stress, sleep, and arousal (motor and sensory) but instead had some similarity with the frontoparietal cognition maps established by task fMRI, making it more interpretable. Altogether, these findings are most consistent with SES acting as a strong confound in BWAS of IQ.

Nongeneralizability of brain-IQ associations across SES strata

For brain-based multivariate models of population variability to be valid, they must not only be replicable and interpretable but also generalize across cohorts (*62*–*65*). Hence, we tested the generalizability of multivariate brain-IQ associations across the SES spectrum. We used canonical correlation analysis (CCA), a common multivariate technique used to learn associations between multivariate brain and nonbrain data, carrying forward hyperparameters from our previous work (*1*) to reduce overfitting.

We tested the generalizability of multivariate brain-IQ score association models in a so-called cross-contextual comparison framework (Fig. 5, RSFC; for cortical thickness, see fig. S19) (*6*). Specifically, we trained brain-based models of IQ scores either on ABCD subsamples covering the full SES spectrum (Fig. 5, A to E, and fig. S19, A to E) or subsamples restricted to either relatively high-SES (Fig. 5, F to J; social and economic domain of the Child Opportunity Index > 0.75) or low-SES (Fig. 5, K to O; social and economic domain of the Child Opportunity Index < −0.54) backgrounds. We subsequently tested the models using the predefined left-out ABCD replication dataset, matched for sample size ($n = 579$) and IQ distribution (see Fig. 5, A to O; fig. S19 for cortical thickness; and Materials and methods). In both cases, the SES spectrum was truncated in the training data (Fig. 5, I and N) but not the test data (Fig. 5, J and O). As a baseline, the multivariate model trained on children from the full SES spectrum achieved an association of $r_{oos} = 0.30$ in the test subsample ($P < 0.001$; Fig. 5A; see fig. S19 for cortical thickness and figs. S20 and S21 for CPM). However, the model trained on only higher-SES children did not generalize out of sample (IQ-matched), with an $r_{oos} = 0.01$ ($P = 0.45$; Fig. 5F). Conversely, the model trained on only lower-SES children (IQ-matched) achieved a strong association of $r_{oos} = 0.30$ in the test subsample ($P < 0.001$; Fig. 5K). Repeating these analyses with cortical thickness generated the same results (fig. S19). The poor generalizability of brain-IQ associations when models were trained on individuals from high- but not low-SES backgrounds suggests a nonlinear dependence of brain-IQ associations on SES.

SES shortcut learning in brain-IQ associations

To determine why IQ BWAS generalizability plummeted as subsamples became more restricted to higher-SES children, we implemented a

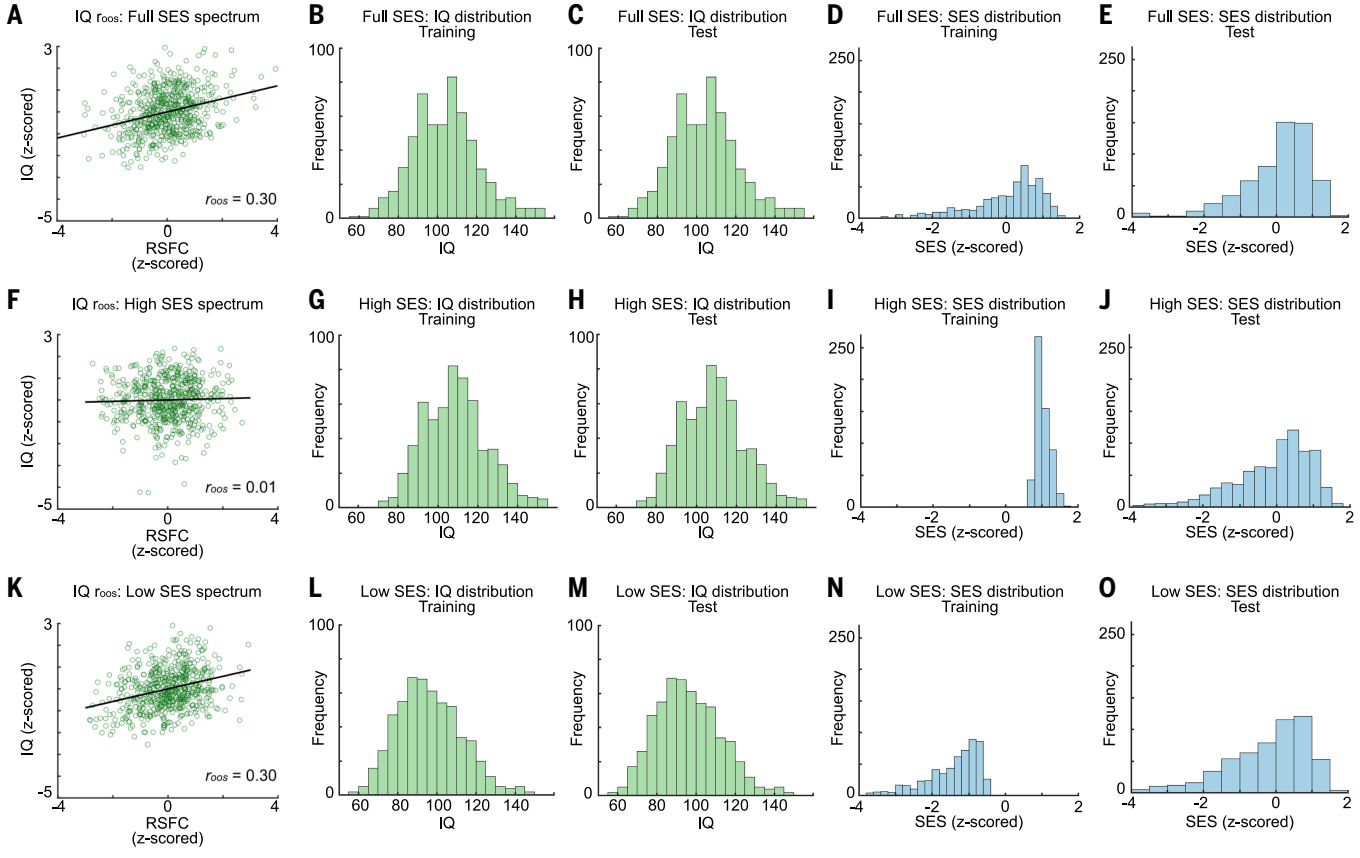

Fig. 5. Testing the generalizability of multivariate brain-IQ score associations. (**A**) Out-of-sample IQ (NIH Toolbox Cognition Battery, all subscales) associations from RSFC (333 parcels; see fig. S19 for cortical thickness), using CCA, in the ABCD Study. The *y* axis shows the first canonical variates for IQ in the test data, scaled by training weights. The *x* axis shows the same for RSFC. The correlation between the first canonical variates for IQ and RSFC is out-of-sample relative to the training data (r_{oos}). Training and test sets were subsampled ($n = 579$) from the predefined discovery ($n = 2316$) and replication ($n = 2263$) samples, respectively, covering the full SES (social and economic domain of the Child Opportunity Index) spectrum. Subsample multivariate associations ($r_{oos} = 0.30$; $n = 579$) were weaker than in the full sample ($r_{oos} = 0.35$; $n = 2316$) because effect sizes scale with *n* (*125*). (**B** and **C**) IQ (green) distribution was matched in the training (B) and test (C) sample. (**D** and **E**) SES (blue) distributions were likewise similar in the training (D) and test (E) sample. (**F**) Out-of-sample IQ score with RSFC association, as in (A), but for a size-matched ($n = 579$) training subsample drawn from only the high-SES spectrum ($z > 0.75$). (**G** and **H**) IQ distribution in the training sample (high SES only) (G) was matched to the test sample (full SES range) (H). (**I** and **J**) This restricted the training SES distribution (I) to high, but not for the test sample (J). (**K**) Out-of-sample IQ score with RSFC association, exactly as in (A), but for a size-matched ($n = 579$) training subsample drawn from only the low-SES spectrum ($z < -0.54$). (**L** and **M**) IQ distribution in the training sample (low SES only) (L) was matched to the test sample (full SES range) (M). (**N** and **O**) This restricted the training SES distribution (N) to low, but not for the test sample (O).

finer-grained cross-contextual analysis (*6*). We continuously varied the SES composition of the training sample, starting with children from only high-SES backgrounds, and gradually moved to include the full SES spectrum. These models were then tested on the full replication sample (Fig. 6A) while tracking the correlation (r_{vars}) between SES and IQ. As training samples progressed from most SES restricted (high only) to least restricted, multivariate subsample RSFC associations increased from $r_{oos} = 0.03$ to $r_{oos} = 0.23$ (Fig. 6A; see fig. S22A for cortical thickness; $r_{oos} = 0.02$ to $r_{oos} = 0.16$). Paralleling this trajectory, the correlation between SES and IQ in the training subsamples increased from $r_{vars} = 0.08$ in high-SES subsamples to $r_{vars} = 0.31$ when subsampling the full cohort (Fig. 6B; see fig. S22B for cortical thickness). RSFC and cortical thickness–based models of IQ only generalized when the correlation between SES and IQ was at least $r_{vars} > 0.10$. Even when IQ BWAS models successfully generalized, models trained on brain-IQ associations performed better [larger out-of-sample correlation (r_{oos})] when tested on SES compared with IQ (Fig. 6C, RSFC; see fig. S22C for cortical thickness). Thus, when multivariate models of brain-IQ associations appear to generalize, they do so by learning the shortcut (SES) better than the intended target (IQ). Family income and parental education (family-level socioeconomic variables) also had strong correlations with IQ scores ($r_{vars} = 0.34$ for both). Varying the training sample by family income or parental education also reduced multivariate associations but less than for SES (fig. S23). This suggests that neighborhood-level socioeconomic variables have a particularly strong effect on brain-IQ associations.

To test whether brain-based associations of SES were more robust than those for IQ, we evaluated multivariate models (Fig. 6D for RSFC; fig. S22D for cortical thickness) by training them on ABCD subsamples ranging from high IQ (NIH Toolbox Cognition Battery, total score > 110) only (Fig. 6D, left, solid line; see fig. S22D for cortical thickness) to the full IQ spectrum in ABCD (Fig. 6D, right, solid line; see fig. S22D for cortical thickness). Across all sample compositions (Fig. 6D, *x* axis), generalizability remained greater for brain-based models of SES (all $r_{oos} > 0.20$; Fig. 6D, solid blue line) than IQ (Fig. 6A, solid green line). Even when the correlation between SES and IQ had been reduced to $r_{vars} < 0.10$ (Fig. 6B; see fig. S22B for cortical thickness), association strength remained high (Fig. 6, D and E, all $r_{oos} > 0.20$; fig. S22, C and D, all $r_{oos} > 0.15$), despite a truncated SES distribution (fig. S24). Moreover, SES associations remained unchanged when varying the

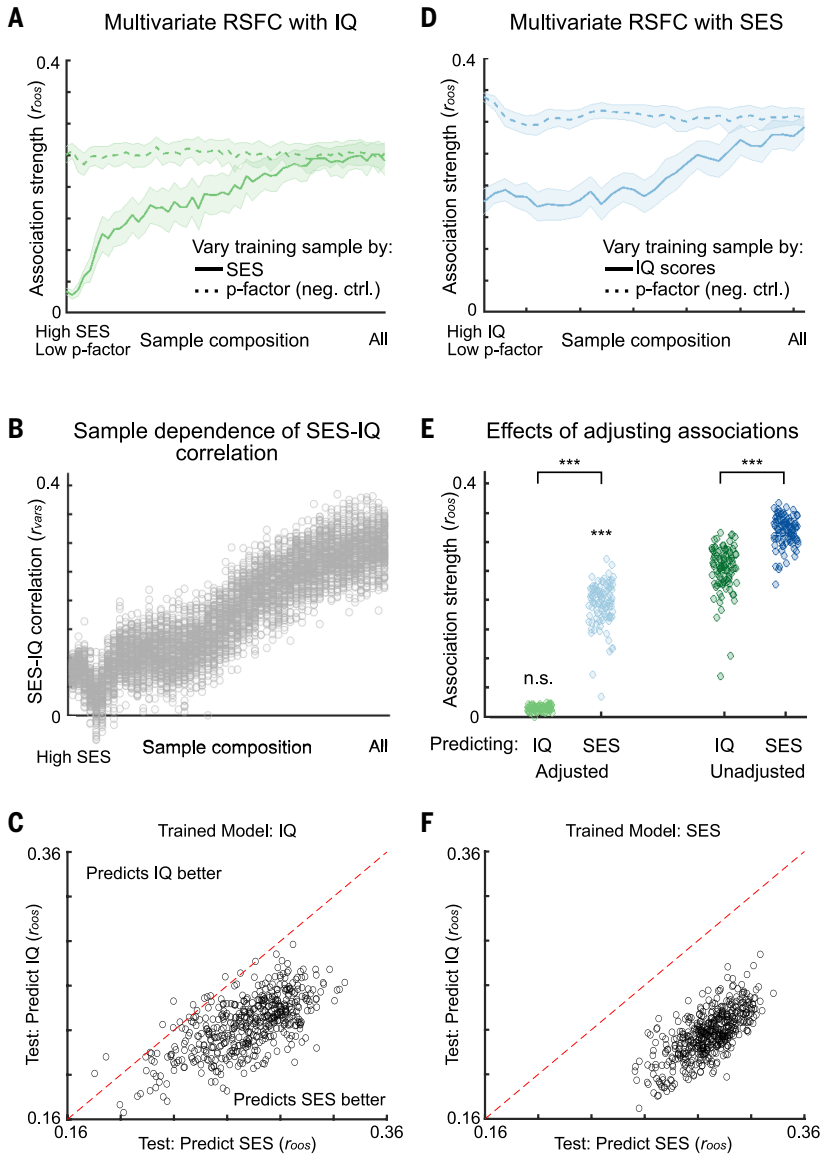

Fig. 6. Cross-contextual analyses testing for shortcut learning in multivariate brain associations with IQ and SES. (**A**) Out-of-sample IQ (NIH Toolbox Cognition Battery, all subscales) with RSFC association, using CCA, in the ABCD Study (baseline; as in Fig. 5), with training data of varying compositions. Discovery ($n = 2316$; training) data were repeatedly subsampled ($n = 500$) based on SES (solid line), to range from high SES only (left) to the full range (right); as a negative control, data were also subsampled based on p-factor (dashed line). Multivariate associations (r_{oos}) are from the replication sample ($n = 2263$; test set; *y* axis); line shading indicates SDs (100 bootstraps). (**B**) Correlations between SES and IQ (r_{vars}; *y* axis) as a function of subsample SES composition. (**C**) Multivariate models (ridge regression) trained to predict IQ from RSFC in subsamples ($n = 500$) of the discovery data (500 bootstraps). Each model was tested in the full replication sample and used to either predict IQ (*y* axis) or SES (*x* axis). (**D**) Out-of-sample SES (social and economic domain of the Child Opportunity Index, all subscales) with RSFC association, using CCA [as in (A)], with training data of varying IQ (solid line; high IQ on left), and as a control p-factor (dashed line), compositions. (**E**) Multivariate associations (r_{oos}) of RSFC with IQ (green) and SES (blue) from models trained on subsamples ($n = 579$) of the discovery sample, either adjusted (left; light green and blue) or unadjusted (right; dark green and blue) for each other. ***$P < 0.001$, Bonferroni-corrected ($P > 0.05$). (**F**) Same as (C), but for models trained on RSFC with SES associations. In (C) and (F), red dashes show the identity line.

training sample by genetic ancestry (fig. S25 and Materials and methods). Thus, unlike brain-IQ associations, which did not generalize ($r_{oos} = 0.01$, $P = 0.43$; Fig. 6E) without a correlation (r_{vars}) with SES, multivariate brain-SES associations remained strong ($r_{oos} = 0.19$, $P = 2.54 \times 10^{-23}$; Fig. 6E; see fig. S22 for cortical thickness). Models trained on brain-SES associations always performed better [larger out-of-sample correlation (r_{oos})] when tested on the intended SES target compared with when they were tested on IQ (Fig. 6F; see fig. S22F for cortical thickness), thus lacking evidence of shortcut learning.

IQ models trained on children from high-SES backgrounds in the ABCD sample (left-most side of Fig. 6A, *x* axis) also exhibited low generalizability to the Human Connectome Project (HCP) ($n = 877$ individuals, aged 22 to 35 years) dataset (fig. S26; $r_{oos} = 0.03$). ABCD training models increasingly included children from lower-SES backgrounds, and generalizability to the HCP sample similarly improved (fig. S26; $r_{oos} \sim 0.20$).

As a negative control, we also varied the training sample composition by psychopathology (p-factor; Fig. 6A, dashed green line), when predicting IQ scores (Fig. 6A) and SES (Fig. 6D, dashed blue line) from RSFC data. Stratification of the training samples by psychopathology (Fig. 6, A and D, left, low p-factor, dashed lines) had no effect on IQ and SES association generalizability. As another negative control, we also showed that multivariate brain-based associations generalized across sexes by training on female children and testing on males ($r_{oos} = 0.31$) and vice versa ($r_{oos} = 0.29$) (for IQ, see fig. S27; see fig. S28 for SES generalizability across sex).

Thus, the generalizability of multivariate brain-based (RSFC and cortical thickness) association models with IQ varies with SES, independent of analytic approach (Fig. 5, Fig. 6, figs. S19 to S23, and figs. S25 to S28). In samples restricted to children with high SES, in which only a negligible or weak correlation between SES and IQ scores existed ($r_{vars} < 0.10$), out-of-sample brain-IQ associations were small ($r_{oos} < 0.10$; Fig. 5F; Fig. 6A, solid green line, left side of plot; and Fig. 6E). Seeming generalization of IQ BWAS models was driven by shortcut learning of SES instead of IQ associations.

The socioeconomic brain pattern

Brain associations with SES were found in the motor and sensory regions, in a pattern most similar to that of norepinephrine receptors, sleep correlates tracked with EEG, and the effects of high-dose methylphenidate (Fig. 3). Significant overlap between the SES and neurotransmitter maps was specific to norepinephrine ($P = 0.002$); no other neurotransmitter maps were similar to SES (all $P > 0.05$; table S2).

Similar to SES, sleep, screen time, and IQ BWAS maps were patterned onto early motor and sensory regions. This network pattern, present in RSFC data, does not correspond to brain regions active during complex cognitive operations (FPN) (Figs. 2 and 3) (*47*), such as manipulating information held in working memory (Fig. 3). Rather, this network pattern exhibits the greatest day-to-day variability (*9*) within an individual and changes with drastic motor interventions (*66*), sleep deprivation (*19*), caffeine intake (*17*, *67*), length of day (seasonal effects) (*68*), and stimulant use (Fig. 3 and fig. S29), which demonstrates its environmental sensitivity. Given that an individual's environmental exposures have powerful effects on the brain's neuroendocrine system (*69*), the observed principal BWAS map may be representing a biological pathway through which socioeconomics is becoming biologically

embedded through differences in sleep quality (*70*), chronic physiological stress (*71*), and screen use [in particular social media (*72*)]. To give credence to this abductive argument, we compiled a composite of stress in the ABCD Study using measures established previously (*73*) related to abuse, household challenges, and neglect (Materials and methods). The correlation between the stress RSFC brain map pattern and the SES pattern was $r_{patterns} = 0.50$ ($P < 0.001$, spin test). Thus, the SES brain pattern may reflect the direct effects of childhood sleep deprivation and stress as well as responsive adaptations. Although the developing brain adjusts to its environment, socioeconomic brain patterns similar to those associated with detrimental factors, such as insufficient sleep (*74*) and chronic stress (*71*), are unlikely to be adaptive longer term.

Childhood poverty is correlated with poorer physical and mental health outcomes, lower lifetime earnings, and decreased life expectancy (*75*–*78*). Gaining deeper insight into modifiable variables through which SES affects brain development (*79*) is critically important. In addition to sleep and screen time, there are numerous other pathways through which socioeconomics likely affect brain development as well as cognitive and psychiatric outcomes (*80*, *81*). Neighborhood contributions capture individual differences in many potentially influential factors, such as schools (*82*), threat and crime (*83*), and access to health care (*84*). Other pathways include nutrition (*85*), physiological stressors (*86*, *87*), inflammation (*88*), and pollution (*89*).

Reification of IQ into the brain

One goal of inquiries into the neurobiological basis of IQ has been to attribute specific and generalizable predictive power to brain features that explain individual differences in IQ scores. Generalizability of brain-based IQ models required including children with lower SES (Fig. 5, Fig. 6A, fig. S19, and fig. S22A). Machine learning techniques, although powerful and more sensitive than univariate approaches, can detect associations outside of the target variable (in this case, IQ) that lack generalizability, replicability, or practicality (*90*). In medical applications, machine learning has generated invalid findings by learning background information of images related to lungs with COVID-19, breast cancer, and cell types instead of the target variables (*91*), a phenomenon known as shortcut learning (*92*). Similarly, in this case, brain-based multivariate models of IQ were dependent on the sample's socioeconomic background. This suggests that, similar to previous work in medical imaging, multivariate brain-based models are learning socioeconomic background as a shortcut rather than the intended target of IQ.

BWAS of IQ highlight the importance of taking the effects of childhood socioeconomics into consideration. The generalizability of brain-IQ associations was dependent on socioeconomics, similar to the Scarr-Rowe effect in genetics, where the heritability of IQ is dependent on an individual's SES (*93*). In BWAS, brain-IQ associations did not generalize when models were trained on only higher-SES individuals, despite a typical distribution of IQ scores. This finding, along with previous studies (*94*), calls into question the degree to which IQ scores measure a stable, essentialized trait. Among immigrants, IQ scores within individuals increased with time lived in the US (*95*). Moreover, IQ scores are higher for individuals adopted out of institutional care compared with those who were not (*96*). IQs also increased over much of the 20th century (Flynn effect) (*97*). However, population estimates of IQ in many developed countries peaked in the late 20th century, subsequently reversed (*98*, *99*), and can be explained by environmental causes (*99*).

Environment matters most for a child's brain

The socioeconomic opportunities provided by a child's environment are associated with brain function and structure more than any other variable examined, which suggests that it captures the principal vector of the exposome, along which lived experience manifests in brain organization. Despite having the strongest effect sizes, SES still only explained a subset of brain differences across children (at maximum, 16% with multivariate approaches). It also remains unclear when strong associations between the brain and SES first emerge or when environmental interventions may be most beneficial. Population-level effects cannot predict future outcomes of an individual child. Socioeconomic opportunity is not destiny.

Leading candidates for cost-effectively and rapidly bolstering brain function and structure may be lifestyle interventions related to sleep and chronic stress. Within-person, longitudinal clinical trials are needed to test for robust developmental benefits of sleep and physiological stress interventions. The association patterns between IQ and primary motor and sensory regions indicate that prior brain-IQ correlations may have been driven by physiological stressors related to lower SES (Fig. 3). Claims of IQ tests measuring essentialized intelligence are not neurobiologically grounded. Although correlational, the BWAS maps, bolstered by the neurobiological reference maps, nonetheless highlight the great power of environmental stressors and deprivation, further adding to the worry voiced by Charles Darwin that "if the misery of the poor not be caused by the laws of nature, but by our institutions, great be our sin" [(*100*), p. 608].

Materials and methods

Nonimaging variables and neuroimaging (RSFC, cortical thickness) data were from the ABCD (5.1 release; Fast Track Release 3165 collection) dataset (baseline: $n = 4579$ individuals, aged 9 to 10 years; year 2: $n = 2363$ individuals, aged 11 to 12 years), the HCP [1200 Subjects Data Release (*101*)] dataset ($n = 877$ individuals, aged 22 to 35 years; see below), and the UK Biobank dataset ($n = 32{,}572$ individuals, aged 40 to 69 years; see below) (*8*).

ABCD Study dataset

The ABCD Study obtained centralized institutional review board (IRB) approval from the University of California, San Diego. Each of the 21 sites also obtained local IRB approval. Ethical regulations were followed during data collection and analysis. Parents or caregivers provided written informed consent, and children gave written assent.

We used ABCD Study data from the baseline (9 to 10 years old) sample in all primary analyses. Univariate associations between RSFC and nonimaging variables were replicated using data from the year 2 wave of ABCD Study (see below). For primary analyses leveraging the baseline ABCD sample, RSFC and cortical thickness data from $n = 10{,}259$ participants were obtained through the ABCD fast track portal. To obtain the final sample size, children from the full behavioral sample ($n = 11{,}878$) were first divided into a discovery ($n = 5939$) and replication ($n = 5939$) set, which were previously matched (*41*) across nine variables using the ABCD 3.0 data release: site location, age, sex, ethnicity, grade, highest parental education, handedness, combined family income, and exposure to anesthesia. Family members (sibling pairs, twins, and triplets) were kept together in the same set, and the two sets were matched to include equal numbers of single participants and family members. Refer to fig. S30 for a consort diagram of the datasets.

For supplementary analyses using year 2 ABCD Study data (aged 11 to 12 years), RSFC data from $n = 5386$ participants were obtained through the ABCD fast track portal. Phenotypic assessments collected in year 2 along with the linked external data from the baseline sample were used for replication of effect sizes (384 variables in total, as not all variables collected in the baseline wave were also collected in year 2).

ABCD MRI acquisition

Imaging for each ABCD youth was performed across 21 sites within the US, harmonized across Siemens Prisma, Philips, and GE 3T scanners. Details on image acquisition can be found in Casey *et al.* (*102*).

Twenty minutes of eyes-open (passive crosshair viewing) resting-state data were presented to ensure at least 5 min of low-motion data. All resting-state scans were acquired using a gradient-echo EPI sequence (TR = 800 ms, TE = 30 ms, flip angle = 90°, voxel size = 2.4 mm^3, 60 slices). Head motion was monitored online using Framewise Integrated Real-time MRI Monitoring (FIRMM) software at Siemens sites (*103*).

Neuroimaging data processing overview

We outline the data processing steps here. For further details on the full processing stream, see Feczko *et al.* (*41*). The ABCD-HCP pipeline comprises six stages: (i) PreFreeSurfer, which normalizes anatomical data; (ii) FreeSurfer, which constructs cortical surfaces from the normalized anatomical data; (iii) PostFreeSurfer, which converts outputs from FreeSurfer to CIFTIs and transforms the volumes to a standard volume space using ANTs nonlinear registration; (iv) "Vol" stage, which performs the atlas transformation, mean field distortion correction, and resampling to 2-mm isotropic voxels in a single step using FSL's applywarp tool; (v) "Surf" stage, which projects the volumetric functional data onto the surface; and (vi) "DCANBOLDproc," which performs functional connectivity processing.

DCANBOLDproc includes a respiratory filter to improve framewise displacement (FD) estimates calculated in the vol stage. Second, temporal masks were created to flag motion-contaminated frames using the improved FD estimates (*104*). Frames with FD > 0.30 mm were flagged as motion-contaminated. After computing the temporal masks for high motion frame censoring, the data were processed with the following steps: (i) demeaning and detrending and (ii) interpolation across censored frames using least squares spectral estimation of the values at censored frames (*105*) so that continuous data can be (iii) denoised via a GLM, including whole brain, ventricular, and white matter signals, as well as their derivatives. Denoised data are then passed through (iv) a band-pass filter (0.008 Hz < f < 0.10 Hz) without reintroducing nuisance signals (*106*) or contaminating frames near high motion frames (*107*).

For each participant, RSFC matrices were created by correlating the average time series of BOLD activity within each of 333 cortical regions of interest (ROIs) or parcels (*108*) after discarding frames with a filtered FD > 0.08 mm. For each participant, cortical thickness was extracted from 59,412 cortical vertices.

HCP dataset

For supplementary analyses (fig. S26), we used data from $n = 877$ individuals from the HCP 1200 Subject Data Release (aged 22 to 35 years). All HCP participants provided informed consent. A custom Siemens SKYRA 3.0T MRI scanner and a custom 32-channel head coil were used to obtain high-resolution T1-weighted (MP-RAGE, $TR = 2.4$ s, 0.7 mm^3 voxels) and BOLD contrast sensitive (gradient-echo EPI, multiband factor 8, $TR = 0.72$ s, 2 mm^3 voxels) images from each participant. The HCP used sequences with left-to-right (LR) and right-to-left (RL) phase encoding, with a single RL and LR run on each day for 2 consecutive days for a total of four runs. MRI data were preprocessed as previously described (*1*). All HCP data are available at https://balsa.wustl.edu/.

UK Biobank dataset

For supplementary analyses (figs. S7 and S29), we used preprocessed resting-state data from $N = 32{,}572$ individuals from the January 2020 UK Biobank release (*109*). A 3-tesla Siemens Skyra scanner (Siemens Healthineers, Erlangen, Germany) and a custom 32-channel head coil were used to obtain high-resolution T1-weighted (MP-RAGE, $TR = 2.0$ s, 1.0 mm^3 voxels) and BOLD contrast sensitive (gradient-echo EPI, multiband factor 8, $TR = 0.735$ s, 2.4 mm^3 voxels) images from each participant. For a complete description of study flow and imaging protocols, see Littlejohns *et al.* (*8*). The UK Biobank collects measures of fluid intelligence and income, which we used to correlate with RSFC, mimicking the ABCD.

For additional details related to MRI acquisition and processing for ABCD and HCP data, see Marek *et al.* (*1*). In each dataset (HCP, ABCD, and UK Biobank), we extracted the time series from the 333 cortical ROIs, correlated and Fisher *z*-transformed them.

Head motion can systematically bias developmental studies (*104*, *110*), as well as those relating RSFC to behavior (*110*). However, these systematic biases can be addressed through rigorous head motion correction (*105*). Therefore, we used strict inclusion criteria with regard to head motion in the current study. Specifically, inclusion criteria for the current project [see Casey *et al.* (*102*) for broader ABCD inclusion criteria] consisted of at least 365 frames (5 min) of low-motion (FD < 0.08 mm) RSFC data in the ABCD dataset (8 min of FD < 0.20 for HCP). Based on these criteria, our final baseline ABCD dataset consisted of data from a total of $n = 4579$ youth across the discovery (ARM 1; $n = 2316$) and replication (ARM 2; $n = 2263$) sets. The final 2 year follow up ABCD dataset (year 2) consisted of RSFC data from $n = 2363$ individuals.

Phenotypic assessment

In ABCD, we assessed 649 variables, spanning 12 categories: socioeconomics, screen time, cognition, demographics, physical health, mental health, culture and/or environment, social adjustment, substance use, parenting, personality, and medical history.

The nonimaging variables were selected for consistency with prior genetic phenome-wide association studies (PheWAS) (*40*). In this preceding study, all released ABCD variables were reviewed for inclusion according to: (i) relevance (removal of administrative items, such as measurement device) and (ii) redundancy, resulting in 869 variables. When applicable, missing data were recoded to 0 (such as questions about substance use that remained unasked after a response that the child had not heard of the substance). Otherwise, all missing values were coded as missing (e.g., distress related to the presence of psychotic-like experiences was coded as missing in participants who reported no psychotic-like experiences). All data were triple checked by multiple investigators for relevance, variability, and accurate recoding. Owing to the large BWAS samples needed to establish robust effect size estimates, the variables were further filtered for missingness and frequency variability, such that continuous phenotypes were required to have $n \geq 2000$ participants with nonmissing values. Categorical variables were required to have $n \geq 2000$ endorsements. These requirements resulted in the final total of 649 variables.

A complete list of variables and their effect size rank can be found in table S1. The measures included in each domain are briefly summarized below.

Socioeconomic: We used measures from the census tract produced by the Linked External Data (LED) Environmental workgroup (*111*) and family income to estimate socioeconomics. Family income includes wages, benefits, and child support payments. The LED incorporates the use of geospatial location data to assess individual, neighborhood, and state resolution data based on the child's residential (census tract) location. See Fan *et al.* (*111*) for a detailed description of the LED. Notable linked datasets include the Area Deprivation Index, the Child Opportunity Index, and the Opportunity Atlas.

Screen time: Caregiver- and youth-reported screen time metrics were included. The questionnaires ask about time spent on screens for various types of media, separated for weekdays and weekend days, as well as the frequency of certain screen media activities.

Cognition: All available age-corrected summary scores from the NIH Toolbox Cognition Battery were included, as were summary scores for the Little Man Task and Rey Auditory Verbal Learning Task. Matrix Reasoning and the Cash Choice Task measures were also included.

Demographics: Caregiver-reported demographic variables, such as education, employment, marital status, among others, were included. Family income was also obtained and was categorized as a socioeconomic variable.

Culture and/or environment: Cultural and environmental variables included the neighborhood safety and environment, and youth prosocial behavior; and school risk and protective factors; and neighborhood environment measures as assessed on the residential history derived scores, such as concentrations of lead, ozone, and other toxins.

Physical health: Physical health measures consisted of caregiver-reported sleep disturbances, youth- and caregiver-reported pubertal development, traumatic brain injury information, sports and activities involvement, and anthropometrics (birth weight, height, weight, and waist circumference).

Mental health: Mental health consists of items reflecting family history and caregiver symptoms and behaviors, as well as child symptoms and behaviors. Measures included the CBCL, Brief Problem Monitor-Teacher Report, Prodromal Psychosis Scale, the General Behavior Inventory-Mania, Resilience, and the Bis/Bas System Scales. The KSADS-5 was also administered.

Social adjustment: Social adjustment consists of questionnaires related to peer influence, resilience, socialization, discrimination, and social influence and understanding.

Substance use: Youth self-reported substance familiarity and use patterns, as well as intention to use, subjective response to various substances, and peer use patterns were assessed. Further, objective measures of use, including breathalyzer, nicalert, hair tests, and other toxicology tests are available for all or a subset of participants. Finally, measures of parental rules about substance use and community risk and protective factors were also assessed.

Personality: Personality was assessed by a caregiver report using the Urgency-Premeditation-Perseverance-Sensation Seeking-Positive Urgency (UPPS-P) scale.

Parenting: Youth- and caregiver-reported family environment scale, youth-reported parental monitoring, children's report of parental behavior inventory.

Medical history: Medical history measures consisted of variables related to medical history (broken bones, emergency room visits), medication inventory, and a developmental history questionnaire, which assesses prenatal, pregnancy, and birth events and exposures, and pubertal hormones (testosterone, estradiol, and DHEA).

Race and genetic ancestry

The National Academies of Sciences, Engineering, and Medicine (NASEM) issued a report providing recommendations on using race, ethnicity, ancestry, and other descriptors of population stratification (*112*). The NASEM report asserts that race does not have any biological basis and emphasizes that researchers not use continental labels (that is, African, European, Asian, Native American, and Oceanian ancestry) or socially constructed racial and ethnic categories in genetics studies (Asian, Black, white, etc.). Similarly, for neuroimaging studies, researchers should not blindly "control for race" in brain-based association studies with nonbrain variables, especially when race and ethnicity are patterned onto said variables (*113*–*115*). We acknowledge the complicated historical and present social and economic backdrop in which race, ethnicity, and SES co-occur.

The current study follows these NASEM recommendations and therefore does not evaluate race and ethnicity as target variables in univariate and multivariate brain association models (*116*, *117*). Genetic ancestry is defined within the context of genetic admixture of specific, idiosyncratic reference populations (in this case, ABCD). Ancestral inference methods [principal components analysis (PCA) in ABCD], although more robust than self-reported race, can still be biased by the sampling process and model parameters (*118*). The UK Biobank is more homogeneous than the ABCD Study with respect to race (95% white British, white Irish, or other white background), therefore it was used for control analyses, which showed that the results held in this type of sample (fig. S7).

To test whether brain SES associations were robust to potential differences in genetic ancestry in the ABCD Study, we varied the training samples in RSFC multivariate models of SES by genetic ancestry (fig. S25). Neither race nor genetic ancestry accounted for the observed socioeconomic effects or brain-wide association patterns (figs. S7 and S25).

Data analysis

All models and data shown in the main text were tested for replication in the independent baseline replication (ARM 2) ABCD sample (*41*).

Manhattan plots

Univariate analyses: We correlated each of the 649 nonbrain variables with each ROI pair (edge) in the RSFC data, separately. This procedure resulted in 55,278 associations between RSFC and each nonimaging variable. The effect sizes of all associations are plotted in Fig. 1C, sorted by the 99th percentile (99% CI) across all brain features within each of the 649 variables. Rankings were highly similar when using the maximum or 95% CI r_{BWAS} as the threshold instead of the 99% CI r_{BWAS} (correlation between 99% CI r_{BWAS} and max rankings = 0.96; correlation between 99% and 95% CI r_{BWAS} rankings = 0.99). For cortical thickness data, we correlated each of the 649 variables with each of the 59,412 cortical vertices (fig. S1C).

Multivariate analyses: In addition to univariate associations, we used ridge regression models ($\alpha = 1.0$), to estimate out-of-sample brain-based (RSFC and cortical thickness, separately) multivariate associations for each of the 649 nonimaging variables (predicted scores versus observed scores). For input brain features, we first conducted a PCA, whereby the number of PCs retaining 20% of the variance were subsequently passed as features into the ridge regression models, carrying this hyperparameter forward from our previous work (*1*, *64*). We replicated the ridge regression findings across a range of brain feature sets [number of brain PCs used in training models ranging from 10 to 90% variance explained in the imaging data (*1*)].

Replication analyses with ComBat and singletons only

Technical differences between scanners used in the ABCD study could contaminate statistical inference (*114*). Because the nonimaging variables considered may be unevenly distributed across sites and scanners, certain effects could be driven artificially by scanner or site differences. Thus, we harmonized RSFC data using the batch-adjustment algorithm ComBat (*119*) and subsequently correlated each life factor with harmonized data to demonstrate high reproducibility of brain-wide association strength rankings to RSFC data that was not harmonized using ComBat (table S1).

Additionally, the ABCD Study contains siblings and twins. We repeated the correlations of life factor associations with the brain using a sample of only singletons to demonstrate high reproducibility of brain-wide association strength rankings to the sample that also included siblings and twins (table S1).

Brain-wide association maps

RSFC network maps of exemplar phenotypes SES (social and economic domain of the Child Opportunity Index), sleep duration, screen time (total screen time usage during the week and weekend), IQ (NIH Toolbox

Cognition Battery, total score), and the p-factor (Child Behavioral Checklist, total score) are plotted in Fig. 2, A and B. Maps were constructed by averaging the absolute value of association strengths (bivariate *r* values) across all edges for each ROI. Each resulting brain network map was subsequently min/max normed, separately within each variable.

Cortical thickness maps for the same 649 variables were generated by projecting the mean bivariate *r* of all cortical vertices within a ROI and variable onto the cortical surface in Workbench Connectome (fig. S5, A and B) (*101*). To quantify the similarity between each brain map, we correlated each brain map with every other brain map [at the edge level for RSFC (Fig. 2C) and vertex level for cortical thickness (fig. S5C)], resulting in a 649 × 649 brain map similarity matrix.

Generation and benchmarking of the principal exposome brain map

We used PCA across all 649 brain maps (edge × variable for RSFC; vertex × variable for cortical thickness) and extracted the scores from the first PC, which represents an orthogonal vector containing the greatest amount of variance shared across all brain maps. Brain maps in Fig. 2D (see fig. S5D for cortical thickness) were constructed by averaging the absolute value of association strengths (bivariate *r* values) across all edges for each ROI (RSFC; all vertices within a ROI for cortical thickness).

We computed the spatial correlation between each brain-wide association map and the principal brain map and subsequently ranked them by their correlation strength with the exposome brain map (see Fig. 2E for RSFC and fig. S5E for cortical thickness).

Network-level associations

ROIs were ascribed to their respective functional networks from Gordon *et al.* (*108*) (Fig. 2F; see fig. S5F for cortical thickness). We performed an independent sample *t* test to determine whether the exposome map exhibited significantly stronger associations with motor and sensory networks than all other networks (associative).

Linear mixed effects modeling of RSFC with SES, sleep, screen time, and IQ

To jointly consider the independent contributions of the strongest BWASs (socioeconomics, total screen time, sleep duration, and IQ scores), we used linear mixed-effects models to determine effect sizes of the aforementioned variables. Figure S12A compares resulting standardized beta values from mixed effect models including all variables, as well as those from independent mixed models (for example, SES modeled separately from sleep duration, screen time, and IQ). All mixed models included fixed effects of age, sex, head motion (mean FD) and random effects of site. Figure S12, B to E, contains the residualized brain maps for each variable in the top row as well as a percent difference map in the bottom row.

Nonimaging variable correlations

We quantified the correlation between exemplar variables strongly related to SES (social and economic domain of the Child Opportunity Index) in fig. S8A, as well as each of the 649 nonimaging variables using bivariate correlations (r_{vars}; fig. S8B).

Pattern-based inference

To derive a functional interpretation for the motor and sensory pattern exhibited by the exposome map, we quantified the similarity of the exposome BWAS map with other strong BWAS maps (SES, IQ), task fMRI maps (working memory, reasoning, and cognitive control) from Neurosynth (*120*), and maps of neurotransmitters from Hansen *et al.* (*49*), EEG (*51*), and stimulants [from on/off methlyphenidate fMRI (*50*)].

Inference on similarity between brain maps was performed using the rotational null model of Vázquez-Rodríguez for parcellated surface maps (*121*) using the NeuroMaps software (*44*). The Vázquez-Rodríguez model accounts for the medial wall of the cortical surface by reassigning missing data to the nearest parcel (*121*). To compare observed similarity of brain maps with a null, the real correlation *r* between two maps across the 333 parcels was first computed. Then 2000 rotational null maps were obtained by computed the correlations between each pair of null maps. Finally, the *P* value was computed for the two-tailed alternative hypothesis of $r \neq 0$ by counting the number of permutations in which $|r| < |r_{null}|$ and dividing by the total number of permutations.

To test the hypothesis that the motor and sensory pattern was significantly different between the task fMRI maps (Fig. 3A, left column) and BWAS (Fig. 3A, middle column) and arousal maps (Fig. 3A, right column), we first quantified the proportion of normalized associations that were spatially located in sensory and motor networks (visual, dorsal motor, lateral motor, auditory) versus all others for each map (Fig. 3B). Next, we submitted these values for each map into a one-way ANOVA, grouping by map type (task fMRI, BWAS, arousal). Because the omnibus test was significant, we performed follow-up *t* tests to test each pair of map types using the Tukey-Kramer implementation in Matlab.

Influence of SES on brain with IQ associations

Univariate RSFC with IQ scores (Fig. 4A; NIH Toolbox Cognition Battery, total score) and cortical thickness with IQ scores (fig. S14A) associations were quantified unadjusted for SES, as well as adjusted for SES (social and economic domain of the Child Opportunity Index). All models used linear mixed effects modeling, covarying for the fixed effects of age, sex, and mean FD (a composite measure of head motion), as well as a random effect of site. The resulting *t* statistic was extracted for each univariate brain feature with IQ scores from unadjusted and adjusted models and plotted as a histogram (Fig. 4A).

Adjusting for SES revealed that 95% of univariate RSFC with IQ score associations decreased when adjusting for SES. To determine whether the brain features (RSFC: edges; cortical thickness: vertices) decreased in a systematic or random manner in their association with IQ scores, we correlated the change in *t* statistics in SES adjusted versus unadjusted models (Fig. 4B, *y* axis; see fig. S14B, *y* axis, for cortical thickness) with the *t* statistics for brain with IQ in unadjusted models (Fig. 4B, *x* axis; see fig. S14B, *x* axis, for cortical thickness).

Adjusting multivariate associations of brain with IQ for SES

Ridge regression was used to assess out-of-sample multivariate association between the brain and IQ scores (NIH Toolbox Cognition Battery, total score). Data were split into two equal halves—a training set and test set—across the full baseline ABCD sample ($n = 4579$) and the following steps were repeated across 100 bootstrapped samples. First, PCA was conducted on the training set RSFC data. Components explaining 20% of between-person variance in RSFC (34 components) were extracted and submitted to the training model. The test set RSFC data were projected into the PC coordinate space of the training RSFC data to avoid leakage. The intercept and beta weights were applied to the testing RSFC data to produce predicted IQ scores. These scores were correlated with the observed IQ scores in the test set, resulting in the out-of-sample multivariate association presented in Fig. 4D for RSFC and fig. S8C for cortical thickness. Twenty percent of brain features were chosen to balance data reduction with maximizing out-of-sample (replication) association strength, a hyperparameter choice made in previous work and carried forward in this case to mitigate model overfitting. Moreover, our prior work (*1*) has shown that reproducible multivariate brain-behavior associations using similar CCA models are maximized by including ~20% of RSFC components.

We repeated the above procedure after regressing SES (social and economic domain of the Child Opportunity Index) from brain components in the replication (test) dataset. In Fig. 4D, we report and compare the out-of-sample multivariate association for RSFC (see fig. S14C

for cortical thickness) with IQ score models adjusting for SES with those unadjusted for SES.

Assessing IQ BWAS maps for SES confounding

One potential explanation for the BWAS IQ map not matching the known pattern of higher-order cognition was that it might be confounded by SES. If SES was confounding brain-IQ associations, then adjusting the BWAS IQ map for SES via linear regression should better align the adjusted BWAS IQ map higher-order cognition, rather than arousal. To test this, we compared the unadjusted and adjusted IQ BWAS maps with arousal (stimulant use: on/off methlyphenidate) and reasoning (Neurosynth) computing the correlation ($r_{patterns}$) of the normalized (min/max) adjusted and unadjusted IQ maps (separately) to each of stimulant use (Fig. 3A, right column) and reasoning (Fig. 3A, left column). SES and IQ adjusted data were carried forward from the resulting beta maps explained in the methods above (see "Linear mixed effects modeling of RSFC with SES, sleep, screen time, and IQ").

Adjusting multivariate associations of brain with SES for IQ scores

Ridge regression was used to assess out-of-sample multivariate association between the brain and SES (social and economic domain of the Child Opportunity Index). Data were split into two equal halves—a training set and test set—across the full baseline ABCD sample (n = 4579) and the following steps were repeated across 100 bootstrapped samples. First, PCA was conducted on the training set RSFC data. Components explaining 20% of between-person variance in RSFC (34 components) were extracted and submitted to the training model. The test set RSFC data were projected into the PC coordinate space of the training RSFC data to avoid leakage. The intercept and beta weights were applied to the testing RSFC data to produce predicted SES scores. These scores were correlated with observed SES in the test set, resulting in the out-of-sample multivariate association presented in fig. S17A for RSFC and fig. S17B for cortical thickness.

The above procedures were repeated after regressing IQ (NIH Toolbox Cognition Battery, total score) from brain components in the replication (test) dataset. In fig. S17A, we report and compare the out-of-sample multivariate association for RSFC (fig. S17B for cortical thickness) with SES models adjusting for IQ scores with those unadjusted for IQ scores.

CPM: Multivariate associations of brain with IQ

The CPM (*60*) was implemented to generate an out-of-sample association between brain function (RSFC; fig. S15) and IQ scores (NIH Toolbox Cognition Battery, total score; fig. S16 for cortical thickness), adjusted for SES (social and economic domain of the Child Opportunity Index) and unadjusted. Out-of-sample association strength (r_{oos}) is reported as the correlation between predicted and observed phenotypic scores (using models trained on the discovery set). We repeated this analysis 100 times on random split-halves of the data. SES was regressed from the observed test set IQ scores before correlating predicted versus observed values for adjusted models (*61*).

Additional deconfounding approaches in multivariate modeling

Regressing confounds from both the training and test datasets can result in either inflated or deflated out-of-sample associations and is not recommended (*61*). For the multivariate models presented in Fig. 4 and fig. S17, in which we controlled for SES when predicting IQ scores from either RSFC or cortical thickness data, we regressed SES in the test sample only. Similarly, in brain-based models of SES, we regressed IQ scores from the test set.

We also performed analyses of multivariate brain-based associations with IQ scores and SES, separately, using a broader form of a confound isolation cross-validation procedure (*61*). We conducted this set of analyses using ridge regression, given a single target phenotype (either IQ scores or SES).

In confound isolation cross-validation (*61*), a test set of data is generated from the full dataset such that the confound, z (in this case SES; social and economic domain of the Child Opportunity Index) and the target, y (in this case IQ; NIH Toolbox Cognition Battery, total score), are uncorrelated. Given the strong correlation between SES and IQ scores in the ABCD data (r_{vars} = 0.31), it is difficult to generate random samples in which the correlation between SES and IQ are close to 0 in larger subsamples. To generate such samples, we relied on a nested cross validation framework consisting of a test set of n = 50. Across 1000 iterations, we randomly selected test samples of n = 50 and extracted the correlation between SES and IQ (fig. S18). Brain-based (RSFC) models of IQ were trained on the remaining n = 4529 participants and then tested on the n = 50 test sample.

Generalizability of multivariate brain with IQ associations: CCA

For all main generalizability analyses, CCA was used. CCA learns associations between multivariate brain and nonbrain data. Hyperparameters were carried forward from our previous work (*1*) to reduce overfitting. Target variables for generalizability analyses included IQ scores (NIH Toolbox Cognition Battery, all subscales) and SES (all subscales of the social and economic domain of the Child Opportunity Index). Generalizability was assessed by training models on subsamples of the baseline ABCD discovery sample (n = 2316) and testing models on the baseline ABCD replication sample (n = 2263; Fig. 5, Fig. 6, fig. S19, figs. S22 to S25, and fig. S27) and the HCP dataset (fig. S26).

Out-of-sample generalizability of multivariate models of RSFC and cortical thickness (separately) with IQ scores (NIH Toolbox Cognition Battery, all subscales) was tested in subsamples with varying SES composition. For these analyses (RSFC: Fig. 5; cortical thickness: fig. S19), we trained models on subsamples of ABCD discovery data (n = 579), that either covered the full SES spectrum, or that were restricted to individuals from higher SES (z-scored social and economic domain of the Child Opportunity Index > 0.75) or lower SES (z-scored social and economic domain of the Child Opportunity Index < −0.54). In all cases, the IQ distributions of the training (discovery) and test (replication) set were matched.

Generalizability of multivariate brain with IQ associations: CPM

Generalizability of brain-based IQ models was also tested using CPM. For CPM analyses, models were trained using random split halves of the full baseline ABCD data containing individuals from only either lower socioeconomic opportunity (z-scored social and economic domain of the Child Opportunity Index < −0.25; n = 579) or higher socioeconomic opportunity (z-scored social and economic domain of the Child Opportunity Index > 0.75; n = 529). These cutoffs were chosen because they are >0.5 SDs from the median z-scored social and economic domain of the Child Opportunity Index value of 0.25. In contrast to CCA, CPM cannot learn associations between two multivariable datasets; therefore, IQ scores (NIH Toolbox Cognition Battery, total score) were used as the target variable. Each model was subsequently tested separately on (i) all individuals in the replication dataset (full), (ii) individuals from lower socioeconomic opportunity neighborhoods (low), and (iii) individuals from high socioeconomic opportunity neighborhoods (high). This 2 × 3 design was used for CPM models of RSFC with IQ scores (fig. S20), and cortical thickness with IQ scores (fig. S21).

Testing for shortcut learning in brain-based models of IQ

SES: Out-of-sample generalizability of multivariate models (CCA) of RSFC with IQ scores (NIH Toolbox Cognition Battery, all subscales), was tested for varying degrees of SES using the ABCD discovery dataset (Fig. 6A) as a training set and either the ABCD replication dataset (Fig. 6A) or the HCP (adult) dataset (fig. S26) as a test set. For supplementary analyses on cortical thickness, see fig. S22. We trained models on subsamples of the ABCD discovery set with varying compositions

with regards to SES (*z*-scored social and economic domain of the Child Opportunity Index), ranging from high (containing only high-SES individuals) to full sample (containing individuals randomly sampled from all degrees of SES), with a total of 54 bins that were bootstrap resampled 100 times for a total of 5400 models. The ABCD discovery training set subsample size was $n = 500$; testing was done on the full ABCD replication dataset. The ABCD discovery training set subsample size was $n = 877$ to match the out-of-sample testing for generalizability analyses on the full HCP sample ($n = 877$; fig. S26). The mean across the 100 bootstrap resamplings ±1 SD is plotted in Fig. 6A and fig. S26. For each of the 5400 models, we quantified the correlation between IQ, the target variable, and SES (Fig. 6B).

Psychopathology: The above analyses regarding the generalizability of multivariate models (CCA) of RSFC with IQ scores within the ABCD dataset, were repeated but rather than varying subsample composition with respect to SES in the ABCD training sample, we varied the magnitude of total psychopathology scores (CBCL total score; p-factor) from low (indicates no psychopathology), to full sample (individuals randomly sampled from the whole p-factor distribution). The ABCD discovery training set subsample size was $n = 500$; testing was done on the full ABCD replication dataset. The mean across the 100 resamples ±1 SD is also plotted in Fig. 6A.

Testing for shortcut learning in brain-based models of SES

IQ: Out-of-sample generalizability of multivariate models (CCA) of RSFC with SES (social and economic domain of the Child Opportunity Index, all subscales), was tested across subsamples with varying degrees of IQ (all individuals in the training subsample range: 80 > IQ > 110, where IQ > 110 was most restrictive) using the ABCD discovery dataset as a training set and the full ABCD replication dataset (Fig. 6D) as a test set. We trained models using ABCD subsamples with varying IQ compositions (NIH Toolbox Cognition Battery, total score), ranging from high IQ only (containing only individuals with IQ > 110) to the full sample (containing individuals randomly sampled from all degrees of IQ), with a total of 31 bins that were bootstrap resampled 100 times for a total of 3100 models. Each discovery training set consisted of $n = 500$ individuals for testing on the full ABCD replication set. The mean across 100 bootstrap resamplings ±1 SD is plotted (Fig. 6D and fig. S25).

Psychopathology: We repeated the above analyses regarding the generalizability of multivariate models (CCA) of RSFC with SES within the ABCD dataset, but rather than varying subsample composition with respect to IQ in the discovery training sample, we varied the degree of total psychopathology (CBCL total score; p-factor) from low (no psychopathology), to full sample (individuals randomly sampled from the whole p-factor distribution). Each discovery training set subsample consisted of $n = 500$ individuals for testing on the full replication set. The mean across the 100 bootstrap resamplings ±1 SD is also plotted (Fig. 6D and fig. S25).

Genetic ancestry: The out-of-sample generalizability of multivariate models (CCA) of RSFC with SES (social and economic domain of the Child Opportunity Index, all subscales) was tested within the ABCD discovery dataset, varying the training subsamples by genetic ancestry. Each ABCD discovery training set consisted of $n = 500$ individuals for testing on the full ABCD replication dataset ($n = 2263$). Genetic ancestry was estimated using genetic PCs, which reflect the population history of the individuals within a sample (*122*). For ABCD, PC-AiR was used in previously published work (*123*) to calculate the genetic PCs, which were extracted from the ABCD 5.1 data release. PC-AiR was used because of the ability to derive population structure from study cohorts with high heterogeneity and related family members (*123*, *124*). Relatively more homogeneous subsamples were generated for each of the 32 PCs by restricting the range of each genetic PC separately. For each PC, a total of 31 bins were bootstrap resampled 100 times to match Fig. 6D. For fig. S25, the average out-of-sample correlation (r_{oos}) across bootstraps was averaged over all 32 PCs. The mean across PCs ±1 SD is plotted in fig. S25.

Additional testing for shortcut learning in multivariate models of IQ and SES

To identify shortcut learning, we evaluated whether multivariate models trained on IQ (NIH Toolbox Cognition Battery, total score) performed better when tested on IQ or SES (social and economic domain of the Child Opportunity Index) in a left-out sample (Fig. 6C; see fig. S22F for cortical thickness). This approach was repeated for multivariate RSFC models trained on SES (Fig. 6F; see fig. S22F for cortical thickness). We used ridge regression, as model weights from CCA cannot be transferred from data with different dimensionality (there exists a different number of subscales on the NIH Toolbox Cognition Battery versus the social and economic domain of the Child Opportunity Index). Multivariate models were trained on RSFC with IQ associations on random subsets ($n = 500$) of the discovery sample (500 bootstraps). Models were subsequently tested on the full replication sample ($n = 2263$) in which the target was either IQ [y axes; out-of-sample correlation (r_{oos}) between predicted and observed IQ scores] or SES (x axis; r_{oos} between predicted and observed SES scores).

Similarly, multivariate models (ridge regression) were trained on RSFC with SES associations on random subsets ($n = 500$) of the discovery sample (500 bootstraps). Models were subsequently tested on the full replication sample ($n = 2263$) in which the target was either IQ (y axes; r_{oos}) or SES (x axis; r_{oos}).

Generalizability of brain with IQ score and SES associations across sexes

To demonstrate specificity of lower generalizability of brain connectivity with IQ score associations as a function of SES, RSFC with IQ models and RSFC with SES models were trained (separately) using either only females or only males in the discovery dataset. Subsequently, each of those models were tested in the replication dataset of either female only or male only (fig. S27). These analyses were repeated for RSFC with SES (social and economic domain of the Child Opportunity Index, all subscales) associations (fig. S28).

Significance testing

Significance testing included both parametric and nonparametric tests. Corrected *P* values were reported where appropriate. All discovery and replication effect sizes were reported in the tables and figures to encourage interpretation of effect sizes over *P* values when using larger ($n > 1000$) population-level datasets.

REFERENCES AND NOTES

1. S. Marek *et al.*, Reproducible brain-wide association studies require thousands of individuals. *Nature* **603**, 654–660 (2022). doi: 10.1038/s41586-022-04492-9; pmid: 35296861
2. J. Chen *et al.*, Shared and unique brain network features predict cognitive, personality, and mental health scores in the ABCD study. *Nat. Commun.* **13**, 2217 (2022). doi: 10.1038/s41467-022-29766-8; pmid: 35468875
3. L. Q. R. Ooi *et al.*, Longer scans boost prediction and cut costs in brain-wide association studies. *Nature* **644**, 731–740 (2025). doi: 10.1038/s41586-025-09250-1; pmid: 40670782
4. T. Spisak, U. Bingel, T. D. Wager, Multivariate BWAS can be replicable with moderate sample sizes. *Nature* **615**, E4–E7 (2023). doi: 10.1038/s41586-023-05745-x; pmid: 36890392
5. E. L. Durham *et al.*, Multivariate analytical approaches for investigating brain-behavior relationships. *Front. Neurosci.* **17**, 1175690 (2023). doi: 10.3389/fnins.2023.1175690; pmid: 37583413
6. S. H. Gage, M. R. Munafò, G. Davey Smith, Causal Inference in Developmental Origins of Health and Disease (DOHaD) Research. *Annu. Rev. Psychol.* **67**, 567–585 (2016). doi: 10.1146/annurev-psych-122414-033352; pmid: 26442667
7. N. D. Volkow *et al.*, The conception of the ABCD study: From substance use to a broad NIH collaboration. *Dev. Cogn. Neurosci.* **32**, 4–7 (2018). doi: 10.1016/j.dcn.2017.10.002; pmid: 29051027

8. T. J. Littlejohns *et al.*, The UK Biobank imaging enhancement of 100,000 participants: Rationale, data collection, management and future directions. *Nat. Commun.* **11**, 2624 (2020). doi: 10.1038/s41467-020-15948-9; pmid: 32457287
9. C. Gratton *et al.*, Functional Brain Networks Are Dominated by Stable Group and Individual Factors, Not Cognitive or Daily Variation. *Neuron* **98**, 439–452.e5 (2018). doi: 10.1016/j.neuron.2018.03.035; pmid: 29673485
10. S. Kharabian Masouleh *et al.*, Influence of Processing Pipeline on Cortical Thickness Measurement. *Cereb. Cortex* **30**, 5014–5027 (2020). doi: 10.1093/cercor/bhaa097; pmid: 32377664
11. E. M. Gordon *et al.*, Precision Functional Mapping of Individual Human Brains. *Neuron* **95**, 791–807.e7 (2017). doi: 10.1016/j.neuron.2017.07.011; pmid: 28757305
12. R. V. Raut *et al.*, Global waves synchronize the brain's functional systems with fluctuating arousal. *Sci. Adv.* **7**, eabf2709 (2021). doi: 10.1126/sciadv.abf2709; pmid: 34290088
13. M. D. Greicius, B. Krasnow, A. L. Reiss, V. Menon, Functional connectivity in the resting brain: A network analysis of the default mode hypothesis. *Proc. Natl. Acad. Sci. U.S.A.* **100**, 253–258 (2003). doi: 10.1073/pnas.0135058100; pmid: 12506194
14. M. D. Fox *et al.*, The human brain is intrinsically organized into dynamic, anticorrelated functional networks. *Proc. Natl. Acad. Sci. U.S.A.* **102**, 9673–9678 (2005). doi: 10.1073/pnas.0504136102; pmid: 15976020
15. B. T. T. Yeo *et al.*, The organization of the human cerebral cortex estimated by intrinsic functional connectivity. *J. Neurophysiol.* **106**, 1125–1165 (2011). doi: 10.1152/jn.00338.2011; pmid: 21653723
16. J. D. Power *et al.*, Functional network organization of the human brain. *Neuron* **72**, 665–678 (2011). doi: 10.1016/j.neuron.2011.09.006; pmid: 22099467
17. T. O. Laumann *et al.*, Functional System and Areal Organization of a Highly Sampled Individual Human Brain. *Neuron* **87**, 657–670 (2015). doi: 10.1016/j.neuron.2015.06.037; pmid: 26212711
18. A. Runyan *et al.*, Effects of Cortisol Administration on Resting-State Functional Connectivity in Women with Depression. *Psychiatry Res. Neuroimaging* **337**, 111760 (2024). doi: 10.1016/j.pscychresns.2023.111760; pmid: 38039780
19. B. T. T. Yeo, J. Tandi, M. W. L. Chee, Functional connectivity during rested wakefulness predicts vulnerability to sleep deprivation. *Neuroimage* **111**, 147–158 (2015). doi: 10.1016/j.neuroimage.2015.02.018; pmid: 25700949
20. S. Mueller *et al.*, Individual variability in functional connectivity architecture of the human brain. *Neuron* **77**, 586–595 (2013). doi: 10.1016/j.neuron.2012.12.028; pmid: 23395382
21. W. W. Seeley *et al.*, Dissociable intrinsic connectivity networks for salience processing and executive control. *J. Neurosci.* **27**, 2349–2356 (2007). doi: 10.1523/JNEUROSCI.5587-06.2007; pmid: 17329432
22. R. W. Emerson, J. F. Cantlon, Early math achievement and functional connectivity in the fronto-parietal network. *Dev. Cogn. Neurosci.* **2**, S139–S151 (2012). doi: 10.1016/j.dcn.2011.11.003; pmid: 22682903
23. M. Assem, I. A. Blank, Z. Mineroff, A. Ademoğlu, E. Fedorenko, Activity in the fronto-parietal multiple-demand network is robustly associated with individual differences in working memory and fluid intelligence. *Cortex* **131**, 1–16 (2020). doi: 10.1016/j.cortex.2020.06.013; pmid: 32777623
24. S. Ducharme *et al.*, Trajectories of cortical thickness maturation in normal brain development — The importance of quality control procedures. *Neuroimage* **125**, 267–279 (2016). doi: 10.1016/j.neuroimage.2015.10.010; pmid: 26463175
25. A. M. Fjell *et al.*, Development and aging of cortical thickness correspond to genetic organization patterns. *Proc. Natl. Acad. Sci. U.S.A.* **112**, 15462–15467 (2015). doi: 10.1073/pnas.1508831112; pmid: 26575625
26. D. Rakesh, S. Whittle, M. A. Sheridan, K. A. McLaughlin, Childhood socioeconomic status and the pace of structural neurodevelopment: Accelerated, delayed, or simply different? *Trends Cogn. Sci.* **27**, 833–851 (2023). doi: 10.1016/j.tics.2023.03.011; pmid: 37179140
27. N. Parker *et al.*, Assessment of Neurobiological Mechanisms of Cortical Thinning During Childhood and Adolescence and Their Implications for Psychiatric Disorders. *JAMA Psychiatry* **77**, 1127–1136 (2020). doi: 10.1001/jamapsychiatry.2020.1495; pmid: 32584945
28. K. A. McLaughlin, D. Weissman, D. Bitrán, Childhood Adversity and Neural Development: A Systematic Review. *Annu. Rev. Dev. Psychol.* **1**, 277–312 (2019). doi: 10.1146/annurev-devpsych-121318-084950; pmid: 32455344
29. A. Di Martino *et al.*, Unraveling the miswired connectome: A developmental perspective. *Neuron* **83**, 1335–1353 (2014). doi: 10.1016/j.neuron.2014.08.050; pmid: 25233316
30. M. E. Thomason *et al.*, Altered amygdala connectivity in urban youth exposed to trauma. *Soc. Cogn. Affect. Neurosci.* **10**, 1460–1468 (2015). doi: 10.1093/scan/nsv030; pmid: 25836993
31. M. P. Herzberg *et al.*, Accelerated maturation in functional connectivity following early life stress: Circuit specific or broadly distributed? *Dev. Cogn. Neurosci.* **48**, 100922 (2021). doi: 10.1016/j.dcn.2021.100922; pmid: 33517108
32. U. A. Tooley, D. S. Bassett, A. P. Mackey, Environmental influences on the pace of brain development. *Nat. Rev. Neurosci.* **22**, 372–384 (2021). doi: 10.1038/s41583-021-00457-5; pmid: 33911229
33. E. McCrory, L. Foulkes, E. Viding, Social thinning and stress generation after childhood maltreatment: A neurocognitive social transactional model of psychiatric vulnerability. *Lancet Psychiatry* **9**, 828–837 (2022). doi: 10.1016/S2215-0366(22)00202-4; pmid: 35926524
34. T. W. Cheng *et al.*, Characterizing the impact of adversity, abuse, and neglect on adolescent amygdala resting-state functional connectivity. *Dev. Cogn. Neurosci.* **47**, 100894 (2021). doi: 10.1016/j.dcn.2020.100894; pmid: 33385788
35. D. Rakesh, N. B. Allen, S. Whittle, Longitudinal changes in within-salience network functional connectivity mediate the relationship between childhood abuse and neglect, and mental health during adolescence. *Psychol. Med.* **53**, 1552–1564 (2023). doi: 10.1017/S0033291721003135; pmid: 34429171
36. D. S. Fareri *et al.*, Altered ventral striatal-medial prefrontal cortex resting-state connectivity mediates adolescent social problems after early institutional care. *Dev. Psychopathol.* **29**, 1865–1876 (2017). doi: 10.1017/S0954579417001456; pmid: 29162189
37. L. S. King *et al.*, A Comprehensive Multilevel Analysis of the Bucharest Early Intervention Project: Causal Effects on Recovery From Early Severe Deprivation. *Am. J. Psychiatry* **180**, 573–583 (2023). doi: 10.1176/appi.ajp.20220672; pmid: 37211832
38. J. L. Luby, J. N. Constantino, D. M. Barch, Poverty and Developing Brain. *Cerebrum* **2022**, cer-04-22 (2022). pmid: 35813304
39. D. Rakesh *et al.*, Unraveling the Consequences of Childhood Maltreatment: Deviations From Typical Functional Neurodevelopment Mediate the Relationship Between Maltreatment History and Depressive Symptoms. *Biol. Psychiatry Cogn. Neurosci. Neuroimaging* **6**, 329–342 (2021). doi: 10.1016/j.bpsc.2020.09.016; pmid: 33454282
40. A. J. Gorelik *et al.*, A Phenome-Wide Association Study (PheWAS) of Late Onset Alzheimer Disease Genetic Risk in Children of European Ancestry at Middle Childhood: Results from the ABCD Study. *Behav. Genet.* **53**, 249–264 (2023). doi: 10.1007/s10519-023-10140-3; pmid: 37071275
41. E. Feczko *et al.*, Adolescent Brain Cognitive Development (ABCD) Community MRI Collection and Utilities. bioRxiv 2021.07.09.451638 [Preprint] (2021). doi: 10.1101/2021.07.09.451638
42. A. Fry *et al.*, Comparison of Sociodemographic and Health-Related Characteristics of UK Biobank Participants With Those of the General Population. *Am. J. Epidemiol.* **186**, 1026–1034 (2017). doi: 10.1093/aje/kwx246; pmid: 28641372
43. A. F. Alexander-Bloch *et al.*, On testing for spatial correspondence between maps of human brain structure and function. *Neuroimage* **178**, 540–551 (2018). doi: 10.1016/j.neuroimage.2018.05.070; pmid: 29860082
44. R. D. Markello *et al.*, neuromaps: Structural and functional interpretation of brain maps. *Nat. Methods* **19**, 1472–1479 (2022). doi: 10.1038/s41592-022-01625-w; pmid: 36203018
45. E. M. Gordon *et al.*, A somato-cognitive action network alternates with effector regions in motor cortex. *Nature* **617**, 351–359 (2023). doi: 10.1038/s41586-023-05964-2; pmid: 37076628
46. J. Ren *et al.*, Parkinson's disease as a somato-cognitive action network disorder. *Nature* **651**, 1030–1038 (2026). doi: 10.1038/s41586-025-10059-1; pmid: 41639440
47. S. Marek, N. U. F. Dosenbach, The frontoparietal network: Function, electrophysiology, and importance of individual precision mapping. *Dialogues Clin. Neurosci.* **20**, 133–140 (2018). doi: 10.31887/DCNS.2018.20.2/smarek; pmid: 30250390
48. A. S. Greene, S. Gao, D. Scheinost, R. T. Constable, Task-induced brain state manipulation improves prediction of individual traits. *Nat. Commun.* **9**, 2807 (2018). doi: 10.1038/s41467-018-04920-3; pmid: 30022026
49. J. Y. Hansen *et al.*, Mapping neurotransmitter systems to the structural and functional organization of the human neocortex. *Nat. Neurosci.* **25**, 1569–1581 (2022). doi: 10.1038/s41593-022-01186-3; pmid: 36303070
50. J. S. Siegel *et al.*, Psilocybin desynchronizes the human brain. *Nature* **632**, 131–138 (2024). doi: 10.1038/s41586-024-07624-5; pmid: 39020167
51. M. Falahpour, C. Chang, C. W. Wong, T. T. Liu, Template-based prediction of vigilance fluctuations in resting-state fMRI. *Neuroimage* **174**, 317–327 (2018). doi: 10.1016/j.neuroimage.2018.03.012; pmid: 29548849
52. S. E. Goodale *et al.*, fMRI-based detection of alertness predicts behavioral response variability. *eLife* **10**, e62376 (2021). doi: 10.7554/eLife.62376; pmid: 33960930
53. B. P. Kay *et al.*, Stimulant medications affect arousal and reward, not attention networks. *Cell* **188**, 7529–7546.e20 (2025). doi: 10.1016/j.cell.2025.11.039; pmid: 41448140
54. P. Domenech, E. Koechlin, Executive control and decision-making in the prefrontal cortex. *Curr. Opin. Behav. Sci.* **1**, 101–106 (2015). doi: 10.1016/j.cobeha.2014.10.007
55. N. P. Friedman, T. W. Robbins, The role of prefrontal cortex in cognitive control and executive function. *Neuropsychopharmacology* **47**, 72–89 (2022). doi: 10.1038/s41386-021-01132-0; pmid: 34408280
56. R. E. Jung, R. J. Haier, The Parieto-Frontal Integration Theory (P-FIT) of intelligence: Converging neuroimaging evidence. *Behav. Brain Sci.* **30**, 135–154 (2007). doi: 10.1017/S0140525X07001185; pmid: 17655784
57. E. Koechlin, X.-J. Wang, in *The Frontal Cortex: Organization, Networks, and Function*, M. T. Banich, S. N. Haber, T. W. Robbins (MIT Press, 2024), chap. 10.
58. A. K. Barbey *et al.*, An integrative architecture for general intelligence and executive function revealed by lesion mapping. *Brain* **135**, 1154–1164 (2012). doi: 10.1093/brain/aws021; pmid: 22396393
59. B. H. Vieira *et al.*, On the prediction of human intelligence from neuroimaging: A systematic review of methods and reporting. *Intelligence* **93**, 101654 (2022). doi: 10.1016/j.intell.2022.101654

60. X. Shen *et al.*, Using connectome-based predictive modeling to predict individual behavior from brain connectivity. *Nat. Protoc.* **12**, 506–518 (2017). doi: 10.1038/nprot.2016.178
61. D. Chyzhyk, G. Varoquaux, M. Milham, B. Thirion, How to remove or control confounds in predictive models, with applications to brain biomarkers. *Gigascience* **11**, giac014 (2022). doi: 10.1093/gigascience/giac014; pmid: 35277962
62. J. A. Ricard *et al.*, Confronting racially exclusionary practices in the acquisition and analyses of neuroimaging data. *Nat. Neurosci.* **26**, 4–11 (2023). doi: 10.1038/s41593-022-01218-y; pmid: 36564545
63. J. Li *et al.*, Cross-ethnicity/race generalization failure of behavioral prediction from resting-state functional connectivity. *Sci. Adv.* **8**, eabj1812 (2022). doi: 10.1126/sciadv.abj1812; pmid: 35294251
64. B. Tervo-Clemmens *et al.*, Reply to: Multivariate BWAS can be replicable with moderate sample sizes. *Nature* **615**, E8–E12 (2023). doi: 10.1038/s41586-023-05746-w; pmid: 36890374
65. B. Tervo-Clemmens, S. Marek, D. M. Barch, Tailoring Psychiatric Neuroimaging to Translational Goals. *JAMA Psychiatry* **80**, 765–766 (2023). doi: 10.1001/jamapsychiatry.2023.1416; pmid: 37314757
66. D. J. Newbold *et al.*, Plasticity and Spontaneous Activity Pulses in Disused Human Brain Circuits. *Neuron* **107**, 580–589.e6 (2020). doi: 10.1016/j.neuron.2020.05.007; pmid: 32778224
67. R. Magalhães *et al.*, Habitual coffee drinkers display a distinct pattern of brain functional connectivity. *Mol. Psychiatry* **26**, 6589–6598 (2021). doi: 10.1038/s41380-021-01075-4; pmid: 33875801
68. R. Zhang, E. Shokri-Kojori, N. D. Volkow, Seasonal effect—An overlooked factor in neuroimaging research. *Transl. Psychiatry* **13**, 238 (2023). doi: 10.1038/s41398-023-02530-2; pmid: 37400428
69. B. S. McEwen, Brain on stress: How the social environment gets under the skin. *Proc. Natl. Acad. Sci. U.S.A.* **109**, 17180–17185 (2012). doi: 10.1073/pnas.1121254109; pmid: 23045648
70. D. C. Jarrin, J. J. McGrath, E. C. Quon, Objective and subjective socioeconomic gradients exist for sleep in children and adolescents. *Health Psychol.* **33**, 301–305 (2014). doi: 10.1037/a0032924; pmid: 23730721
71. B. S. McEwen, Neurobiological and Systemic Effects of Chronic Stress. *Chronic Stress* **1**, 2470547017692328 (2017). doi: 10.1177/2470547017692328; pmid: 28856337
72. J. Haidt, *The Anxious Generation: How the Great Rewiring of Childhood Is Causing an Epidemic of Mental Illness* (Penguin, 2024).
73. E. A. Hoffman *et al.*, Stress exposures, neurodevelopment and health measures in the ABCD study. *Neurobiol. Stress* **10**, 100157 (2019). doi: 10.1016/j.ynstr.2019.100157; pmid: 30949565
74. A. Galván, The Need for Sleep in the Adolescent Brain, *Trends Cogn. Sci.* **24**, 79–89 (2020). doi: 10.1016/j.tics.2019.11.002; pmid: 31780247
75. K. E. Pickett, R. G. Wilkinson, Income inequality and health: A causal review. *Soc. Sci. Med.* **128**, 316–326 (2015). doi: 10.1016/j.socscimed.2014.12.031; pmid: 25577953
76. V. Patel *et al.*, Income inequality and depression: A systematic review and meta-analysis of the association and a scoping review of mechanisms. *World Psychiatry* **17**, 76–89 (2018). doi: 10.1002/wps.20492
77. W. S. Ribeiro *et al.*, Income inequality and mental illness-related morbidity and resilience: A systematic review and meta-analysis. *Lancet Psychiatry* **4**, 554–562 (2017). doi: 10.1016/S2215-0366(17)30159-1; pmid: 28552501
78. N. R. Nowatzki, Wealth Inequality and Health: A Political Economy Perspective. *Int. J. Health Serv.* **42**, 403–424 (2012). doi: 10.2190/HS.42.3.c; pmid: 22993961
79. M. J. Farah, The Neuroscience of Socioeconomic Status: Correlates, Causes, and Consequences. *Neuron* **96**, 56–71 (2017). doi: 10.1016/j.neuron.2017.08.034; pmid: 28957676
80. S. B. Johnson, J. L. Riis, K. G. Noble, State of the Art Review: Poverty and the Developing Brain. *Pediatrics* **137**, e20153075 (2016). doi: 10.1542/peds.2015-3075; pmid: 26952506
81. L. Machlin, A. B. Miller, J. Snyder, K. A. McLaughlin, M. A. Sheridan, Differential Associations of Deprivation and Threat With Cognitive Control and Fear Conditioning in Early Childhood. *Front. Behav. Neurosci.* **13**, 80 (2019). doi: 10.3389/fnbeh.2019.00080; pmid: 31133828
82. N. L. Hair, J. L. Hanson, B. L. Wolfe, S. D. Pollak, Association of Child Poverty, Brain Development, and Academic Achievement. *JAMA Pediatr.* **169**, 822–829 (2015). doi: 10.1001/jamapediatrics.2015.1475; pmid: 26192216
83. N. Kravitz-Wirtz, A. Bruns, A. J. Aubel, X. Zhang, S. A. Buggs, Inequities in Community Exposure to Deadly Gun Violence by Race/Ethnicity, Poverty, and Neighborhood Disadvantage among Youth in Large US Cities. *J. Urban Health* **99**, 610–625 (2022). doi: 10.1007/s11524-022-00656-0; pmid: 35672546
84. K. Fiscella, D. R. Williams, Health disparities based on socioeconomic inequities: Implications for urban health care. *Acad. Med.* **79**, 1139–1147 (2004). doi: 10.1097/00001888-200412000-00004; pmid: 15563647
85. S. E. Cusick, M. K. Georgieff, The Role of Nutrition in Brain Development: The Golden Opportunity of the "First 1000 Days." *J. Pediatr.* **175**, 16–21 (2016). doi: 10.1016/j.jpeds.2016.05.013; pmid: 27266965
86. K. De France, G. W. Evans, G. H. Brody, S. N. Doan, Cost of resilience: Childhood poverty, mental health, and chronic physiological stress. *Psychoneuroendocrinology* **144**, 105872 (2022). doi: 10.1016/j.psyneuen.2022.105872; pmid: 35879139
87. W. Zhang *et al.*, Neuroinflammation in the Amygdala Is Associated With Recent Depressive Symptoms. *Biol. Psychiatry Cogn. Neurosci. Neuroimaging* **8**, 967–975 (2023). doi: 10.1016/j.bpsc.2023.04.011; pmid: 37164312
88. N. M. Jiang, M. Cowan, S. N. Moonah, W. A. Petri Jr., The Impact of Systemic Inflammation on Neurodevelopment. *Trends Mol. Med.* **24**, 794–804 (2018). doi: 10.1016/j.molmed.2018.06.008; pmid: 30006148
89. S. Jakositz *et al.*, Tap-Water Lead Monitoring through Citizen Science: Influence of Socioeconomics and Participation on Environmental Literacy, Behavior, and Communication. *J. Environ. Eng.* **148**, 04022060 (2022). doi: 10.1061/(ASCE)EE.1943-7870.0002055
90. P. Ball, Is AI leading to a reproducibility crisis in science? *Nature* **624**, 22–25 (2023). doi: 10.1038/d41586-023-03817-6
91. S. Dhar, L. Shamir, Evaluation of the benchmark datasets for testing the efficacy of deep convolutional neural networks. *Vis. Inform.* **5**, 92–101 (2021). doi: 10.1016/j.visinf.2021.10.001
92. R. Geirhos *et al.*, Shortcut learning in deep neural networks. *Nat. Mach. Intell.* **2**, 665–673 (2020). doi: 10.1038/s42256-020-00257-z
93. S. Scarr-Salapatek, Race, social class, and IQ. *Science* **174**, 1285–1295 (1971). doi: 10.1126/science.174.4016.1285; pmid: 5167501
94. S. von Stumm, R. Plomin, Socioeconomic status and the growth of intelligence from infancy through adolescence. *Intelligence* **48**, 30–36 (2015). doi: 10.1016/j.intell.2014.10.002; pmid: 26640306
95. R. M. Yerkes, *Psychological Examining in the United States Army* (Surgeon-General's Office, Division of Psychology, 1921).
96. K. L. Humphreys *et al.*, Foster care leads to sustained cognitive gains following severe early deprivation. *Proc. Natl. Acad. Sci. U.S.A.* **119**, e2119318119 (2022). doi: 10.1073/pnas.2119318119; pmid: 36095188
97. J. R. Flynn, Massive IQ gains in 14 nations: What IQ tests really measure. *Psychol. Bull.* **101**, 171–191 (1987). doi: 10.1037/0033-2909.101.2.171
98. J. M. Sundet, D. G. Barlaug, T. M. Torjussen, The end of the Flynn effect?: A study of secular trends in mean intelligence test scores of Norwegian conscripts during half a century. *Intelligence* **32**, 349–362 (2004). doi: 10.1016/S0160-2896(04)00052-2
99. B. Bratsberg, O. Rogeberg, Flynn effect and its reversal are both environmentally caused. *Proc. Natl. Acad. Sci. U.S.A.* **115**, 6674–6678 (2018). doi: 10.1073/pnas.1718793115; pmid: 29891660
100. C. Darwin, *Journal of Researches Into the Geology and Natural History of the Various Countries Visited by H. M. S. Beagle: Under the Command of Captain FitzRoy, R.N., from 1832 to 1836* (Henry Colburn, 1839).
101. D. S. Marcus *et al.*, Human Connectome Project informatics: Quality control, database services, and data visualization. *Neuroimage* **80**, 202–219 (2013). doi: 10.1016/j.neuroimage.2013.05.077; pmid: 23707591
102. B. J. Casey *et al.*, The Adolescent Brain Cognitive Development (ABCD) study: Imaging acquisition across 21 sites. *Dev. Cogn. Neurosci.* **32**, 43–54 (2018). doi: 10.1016/j.dcn.2018.03.001; pmid: 29567376
103. N. U. F. Dosenbach *et al.*, Real-time motion analytics during brain MRI improve data quality and reduce costs. *Neuroimage* **161**, 80–93 (2017). doi: 10.1016/j.neuroimage.2017.08.025; pmid: 28803940
104. J. D. Power, K. A. Barnes, A. Z. Snyder, B. L. Schlaggar, S. E. Petersen, Spurious but systematic correlations in functional connectivity MRI networks arise from subject motion. *Neuroimage* **59**, 2142–2154 (2012). doi: 10.1016/j.neuroimage.2011.10.018; pmid: 22019881
105. J. D. Power *et al.*, Methods to detect, characterize, and remove motion artifact in resting state fMRI. *Neuroimage* **84**, 320–341 (2014). doi: 10.1016/j.neuroimage.2013.08.048; pmid: 23994314
106. M. N. Hallquist, K. Hwang, B. Luna, The nuisance of nuisance regression: Spectral misspecification in a common approach to resting-state fMRI preprocessing reintroduces noise and obscures functional connectivity. *Neuroimage* **82**, 208–225 (2013). doi: 10.1016/j.neuroimage.2013.05.116; pmid: 23747457
107. J. Carp, Optimizing the order of operations for movement scrubbing: Comment on Power et al. *Neuroimage* **76**, 436–438 (2013). doi: 10.1016/j.neuroimage.2011.12.061
108. E. M. Gordon *et al.*, Generation and Evaluation of a Cortical Area Parcellation from Resting-State Correlations. *Cereb. Cortex* **26**, 288–303 (2016). doi: 10.1093/cercor/bhu239; pmid: 25316338
109. K. L. Miller *et al.*, Multimodal population brain imaging in the UK Biobank prospective epidemiological study. *Nat. Neurosci.* **19**, 1523–1536 (2016). doi: 10.1038/nn.4393; pmid: 27643430
110. J. S. Siegel *et al.*, Data Quality Influences Observed Links Between Functional Connectivity and Behavior. *Cereb. Cortex* **27**, 4492–4502 (2017). doi: 10.1093/cercor/bhw253
111. C. C. Fan *et al.*, Adolescent Brain Cognitive Development (ABCD) study Linked External Data (LED): Protocol and practices for geocoding and assignment of environmental data. *Dev. Cogn. Neurosci.* **52**, 101030 (2021). doi: 10.1016/j.dcn.2021.101030; pmid: 34891080
112. National Academies of Sciences, Engineering, and Medicine, *Using Population Descriptors in Genetics and Genomics Research: A New Framework for an Evolving Field* (National Academies Press, 2023).

113. A. C. Wysocki, K. M. Lawson, M. Rhemtulla, Statistical Control Requires Causal Justification. *Adv. Methods Pract. Psychol. Sci.* **5**, 25152459221095823 (2022). doi: 10.1177/25152459221095823
114. N. M. Saragosa-Harris *et al.*, A practical guide for researchers and reviewers using the ABCD Study and other large longitudinal datasets. *Dev. Cogn. Neurosci.* **55**, 101115 (2022). doi: 10.1016/j.dcn.2022.101115; pmid: 35636343
115. C. Cardenas-Iniguez, M. R. Gonzalez, Recommendations for the responsible use and communication of race and ethnicity in neuroimaging research. *Nat. Neurosci.* **27**, 615–628 (2024). doi: 10.1038/s41593-024-01608-4; pmid: 38519749
116. K. A. Bird, J. Carlson, Typological thinking in human genomics research contributes to the production and prominence of scientific racism. *Front. Genet.* **15**, 1345631 (2024). doi: 10.3389/fgene.2024.1345631; pmid: 38440191
117. J. G. Schraiber, M. D. Edge, Heritability within groups is uninformative about differences among groups: Cases from behavioral, evolutionary, and statistical genetics. bioRxiv 2023.11.06.565864 [Preprint] (2024). doi: 10.1101/2023.11.06.565864
118. D. J. Lawson, L. van Dorp, D. Falush, A tutorial on how not to over-interpret STRUCTURE and ADMIXTURE bar plots. *Nat. Commun.* **9**, 3258 (2018). doi: 10.1038/s41467-018-05257-7; pmid: 30108219
119. W. E. Johnson, C. Li, A. Rabinovic, Adjusting batch effects in microarray expression data using empirical Bayes methods. *Biostatistics* **8**, 118–127 (2007). doi: 10.1093/biostatistics/kxj037; pmid: 16632515
120. T. Yarkoni, R. A. Poldrack, T. E. Nichols, D. C. Van Essen, T. D. Wager, Large-scale automated synthesis of human functional neuroimaging data. *Nat. Methods* **8**, 665–670 (2011). doi: 10.1038/nmeth.1635; pmid: 21706013
121. B. Vázquez-Rodríguez *et al.*, Gradients of structure-function tethering across neocortex. *Proc. Natl. Acad. Sci. U.S.A.* **116**, 21219–21227 (2019). doi: 10.1073/pnas.1903403116; pmid: 31570622
122. J. Novembre, M. Stephens, Interpreting principal component analyses of spatial population genetic variation. *Nat. Genet.* **40**, 646–649 (2008). doi: 10.1038/ng.139; pmid: 18425127
123. C. C. Fan, R. Loughnan, S. Wilson, J. K. Hewitt, ABCD Genetic Working Group, Genotype Data and Derived Genetic Instruments of Adolescent Brain Cognitive Development Study® for Better Understanding of Human Brain Development. *Behav. Genet.* **53**, 159–168 (2023). doi: 10.1007/s10519-023-10143-0; pmid: 37093311
124. M. P. Conomos, M. B. Miller, T. A. Thornton, Robust inference of population structure for ancestry prediction and correction of stratification in the presence of relatedness. *Genet. Epidemiol.* **39**, 276–293 (2015). doi: 10.1002/gepi.21896; pmid: 25810074
125. M. A. Schulz, D. Bzdok, S. Haufe, J. D. Haynes, K. Ritter, Performance reserves in brain-imaging-based phenotype prediction. *Cell Rep.* **43**, 113597 (2024). doi: 10.1016/j.celrep.2023.113597; pmid: 38159275

ACKNOWLEDGMENTS

We thank K. Humphries for thoughtful comments on our manuscript. Data used in the preparation of this article were obtained from the ABCD Study (https://abcdstudy.org), held in the NIMH Data Archive (NDA). This is a multisite, longitudinal study designed to recruit more than 10,000 children aged 9 to 10 and follow them over 10 years into early adulthood. The ABCD Study is supported by the National Institutes of Health (NIH) and additional federal partners under award nos. U01DA041048, U01DA050989, U01DA051016, U01DA041022, U01DA051018, U01DA051037, U01DA050987, U01DA041174, U01DA041106, U01DA041117, U01DA041028, U01DA041134, U01DA050988, U01DA051039, U01DA041156, U01DA041025, U01DA041120, U01DA051038, U01DA041148, U01DA041093, U01DA041089, U24DA041123, and U24DA041147. A full list of supporters is available at https://abcdstudy.org/federal-partners.html. A listing of participating sites and a complete listing of the study investigators can be found at https://abcdstudy.org/consortium_members/. ABCD consortium investigators designed and implemented the study and/or provided data but did not necessarily participate in the analysis or writing of this Research Article. This manuscript reflects the views of the authors and may not reflect the opinions or views of the NIH or ABCD consortium investigators. The ABCD data repository grows and changes over time. The ABCD data used in this report came from the ABCD annual release 5.1. DOIs can be found at https://nda.nih.gov/study.html?id=2313. The ABCD data used in this report also came from the fast track data release. The raw data are available at https://nda.nih.gov/edit_collection.html?id=2573. Instructions on how to create an NDA study are available at https://nda.nih.gov/nda/tutorials/creating_an_nda_study. Additional support for this work was made possible from the National Institute of Environmental Health Sciences (NIEHS) grants R01-ES032295 and R01-ES031074. Data were provided, in part, by the HCP; the WU-Minn Consortium (U54 MH091657), funded by the 16 NIH institutes and centers that support the NIH Blueprint for Neuroscience Research; and by the McDonnell Center for Systems Neuroscience at Washington University. This research has been conducted, in part, using data from UK Biobank (www.ukbiobank.ac.uk). UK Biobank is generously supported by its founding funders, the Wellcome Trust and the UK Medical Research Council, as well as the Department of Health, Scottish government; the Northwest Regional Development Agency; British Heart Foundation; and Cancer Research UK. This work used the storage and computational resources provided by the Daenerys Neuroimaging Community Computing Resource (NCCR). The Daenerys NCCR is supported by the McDonnell Center for Systems Neuroscience at Washington University, the Intellectual and Developmental Disabilities Research Center (IDDRC; P50 HD103525) at Washington University School of Medicine, and the Institute of Clinical and Translational Sciences (ICTS; UL1 TR002345) at Washington University School of Medicine. This manuscript is the result of funding in whole or in part by the NIH. It is subject to the NIH Public Access Policy. Through acceptance of this federal funding, NIH has been given a right to make this manuscript publicly available in PubMed Central upon the Official Date of Publication, as defined by NIH. The views expressed are those of the authors and do not necessarily represent the official views of the NIH. **Funding:** This study was supported by NIH grants R00MH121518 (to S.M.), K23MH125023 (to M.R.D.), R01MH139880 (to N.R.K.), R00HD109454 (to R.F.S.), P30ES007048 (to C.C.-I.), U24ES036819 (to C.C.-I.), R25DA059073 (to C.C.-I.), R25DA061824 (to C.C.-I.), R01ES032295 (to M.M.H.), R01ES031074 (to M.M.H.), K23NS123345 (to B.P.K.), U01DA041120 (to D.M.B.), K23DA057486 (to B.T.-C.), K23DA057486 (to B.T.-C.), U1DA041120 (to N.U.F.D.), U01DA041148R (to D.A.F.), U24DA055330 (to D.A.F.), R37MH125829 (to D.A.F.), R01MH096773 (to D.A.F.), R01MH115357 (to D.A.F.), and UL1TR002494 (to D.A.F.); National Science Foundation grant DGE-213989 (to A.J.G.); the Jacobs Foundation (to B.T.-C. and N.U.F.D.); and the Kiwanis Foundation (to N.U.F.D.). **Author contributions:** Conceptualized study design and methodology: S.M., B.T.-C., N.U.F.D.; Data curation, analysis, and code: S.M., M.R.D., N.R.K., R.J.C., A.C.M., J.Mi., A.N.V., V.S., S.E.Pa., A.J.G., T.J.H., S.M.M., B.P.K.; Writing of original draft: S.M., M.R.D., D.A.F., B.T.-C., N.U.F.D. All authors reviewed, provided comments, and edited the final manuscript. **Competing interests:** A.N.V., D.A.F., and N.U.F.D. have a financial interest in Turing Medical, Inc., and may financially benefit if the company is successful in marketing FIRMM motion monitoring software products. D.A.F., A.N.V., and N.U.F.D. may receive royalty income based on FIRMM technology developed at the University of Minnesota and Washington University and licensed by Turing Medical, Inc. D.A.F. and N.U.F.D. are cofounders of Turing Medical, Inc. A.N.V., D.A.F., and N.U.F.D. are inventors on patent 11181599 held by Washington University that covers FIRMM. The authors declare no other competing interests. **Data, code, and materials availability:** Participant-level data from all datasets (ABCD, HCP, and UK Biobank) are openly available pursuant to individual, consortium-level data access rules. Data were provided, in part, by the HCP, WU-Minn Consortium (principal investigators: D. Van Essen and K. Ugurbil; 1U54MH091657), funded by the 16 NIH institutes and centers that support the NIH Blueprint for Neuroscience Research, and by the McDonnell Center for Systems Neuroscience at Washington University. Some data used in the present study are available for download from the HCP (www.humanconnectome.org). Users must agree to data use terms for the HCP before being allowed access to the data and ConnectomeDB; details are provided at https://www.humanconnectome.org/study/hcp-young-adult/data-use-terms. The UK Biobank is a large-scale biomedical database and research resource containing genetic, lifestyle, and health information from half a million UK participants (www.ukbiobank.ac.uk). UK Biobank's database, which includes blood samples, heart and brain scans, and genetic data of the 500,000 volunteer participants, is globally accessible to approved researchers who are undertaking health-related research that is in the public interest. This paper analyzes existing, publicly available data, accessible at https://github.com/netneurolab/hansen_receptors/ (PET receptor maps), https://github.com/neurdylab/fMRIAlertnessDetection (EEG arousal template), and https://github.com/ryraut/arousal-waves (respiratory arousal map). Analysis code specific to this study is available at https://gitlab.com/DosenbachGreene/ses_nature. Code for processing ABCD and UK Biobank data can be found at https://github.com/DCAN-Labs/abcd-hcp-pipeline.

SUPPLEMENTARY MATERIALS

science.org/doi/10.1126/science.aee6213
Supplementary Text; Figs. S1 to S32; Tables S1 and S2; References (*126*–*128*); MDAR Reproducibility Checklist

Submitted 10 December 2025; accepted 22 April 2026

10.1126/science.aee6213

Patterns of brain-wide associations reflect socioeconomics

Scott Marek, Meghan Rose Donohue, Nicole R. Karcher, Caroline P. Hoyniak, Roselyne J. Chauvin, Ashley C. Meyer, John Miller, Andrew N. Van, Anxu Wang, Noah J. Baden, Vahdeta Suljic, Kristen M. Scheidter, Julia Monk, Forrest I. Whiting, Nadeshka J. Ramirez-Perez, Samuel R. Krimmel, Athanasia Metoki, Sarah E. Paul, Aaron J. Gorelik, Timothy J. Hendrickson, Stephen M. Malone, Rebecca F. Schwarzlose, Carlos Cardenas-Iniguez, Megan M. Herting, Steven E. Petersen, Joan Luby, Anita C. Randolph, Michael J. Shanahan, Eric Turkheimer, Benjamin P. Kay, Evan M. Gordon, Timothy O. Laumann, Deanna M. Barch, Damien A. Fair, Brenden Tervo-Clemmens, and Nico U. F. Dosenbach

Science **392** (6803), eaee6213. DOI: 10.1126/science.aee6213

Editor's summary

Brain function and structure are known to be affected by environmental conditions. Marek *et al*. mapped brain-wide association studies (BWAS) of 649 phenotypes and exposures to brain function and structure using imaging data from many sources (see the Perspective by Sisk and Satterthwaite). Across adolescents, neighborhood-level socioeconomics showed the strongest brain-wide association, representing a single exposome pattern that explains 34% of all BWAS variance. In their datasets, the classic brain-IQ association largely disappeared when socioeconomic status was properly accounted for. These results provide valuable insights for understanding the effects of the environment on brain development. —Mattia Maroso